RSSI BASED POSITION ESTIMATION IN ZIGBEE SENSOR NETWORKS

by

Fatih İleri

B.S., Electrical and Electronics Engineering, Bahçeşehir University, 2009

Submitted to the Institute for Graduate Studies in
Science and Engineering in partial fulfillment of
the requirements for the degree of
Master of Science

Graduate Program in Electrical and Electronics Engineering
Boğaziçi University

2013

ACKNOWLEDGEMENTS

It is with immense gratitude that I acknowledge the support and help of my Professor Mehmet Akar throughout this thesis work.

ABSTRACT

RSSI BASED POSITION ESTIMATION IN ZIGBEE SENSOR NETWORKS

Localization in wireless sensor networks is getting more and more important in the recent years, since many applications need to locate the source of incoming measurements as precise as possible. Channel propagation and path loss modelling is the key point in successful position estimation. In this thesis, most popular distance estimation and position estimation methodologies are discussed, as well as the indoor channel models developed so far are presented. A ZigBee based RSSI (Received Signal Strength Indicator) measurement system is designed to collect path loss data with varying distances between the transmitter and the receiver. An empirical indoor channel model for ZigBee sensor networks is developed based on the path loss measurements, and implemented with the discussed position estimation methodologies. Not only the developed path loss model, but also the presented position estimation methodologies are evaluated numerically via simulations.

ÖZET

ZIGBEE ALGILAYICI AĞLARINDA AİŞG TABANLI KONUM ALGILAMA

Birçok uygulamada, alınan ölçüm kaynaklarının mümkün olduğunca doğru tespit edilmesinin gerekliliğinden ötürü kablosuz algılayıcı ağlarında konum tespiti son yıllarda gittikçe önem kazanmıştır. Kanal ve yol kaybı modelleme, başarılı bir konum tespit sistemi tasarımında anahtar rol oynamaktadır. Bu çalışmada, şimdiye kadar geliştirilen kapalı alan kanal modelleri ile en çok kullanılan mesafe tahmini ve konum tahmini algoritmaları incelenmiştir. Değişken alıcı verici arası mesafelerinde yol kaybı verileri toplamak üzere ZigBee tabanlı bir AİŞG (Alınan İşaretin Şiddet Göstergesi) ölçüm sistemi tasarlanmıştır. ZigBee algılayıcı ağları için empirik bir kapalı alan kanal modeli tasarlanmış ve incelenen konum tahmini algoritmalarında kullanılarak konum tespiti gerçeklemeleri yapılmıştır. Tasarlanan kanal modelinin yanısıra incelenen konum tahmini algoritmaları da nümerik olarak benzetim çalışmalarıyla test edilmiştir.

TABLE OF CONTENTS

ACKNOWLEDGEMENTS . . . iii
ABSTRACT . . . iv
ÖZET . . . v
LIST OF FIGURES . . . viii
LIST OF TABLES . . . xi
LIST OF ACRONYMS/ABBREVIATIONS . . . xii
1. INTRODUCTION . . . 1
1.1. Commonly Used Distance Estimation Methodologies . . . 1
1.1.1. RSSI . . . 1
1.1.2. Uplink-Time Difference of Arrival (U-TDoA) . . . 2
1.1.3. Time of Arrival (ToA) . . . 2
1.2. The Organization of the Thesis . . . 3
2. REVIEW OF INDOOR RADIO CHANNEL MODELS AND POSITIONING METHODS . . . 4
2.1. Factors Causing Path Loss . . . 4
2.1.1. Free Space Loss . . . 5
2.1.2. Fading . . . 5
2.1.3. Multipath . . . 5
2.1.4. Refraction . . . 5
2.2. Commonly Used Indoor Channel Path Loss Models . . . 6
2.2.1. Microcell Path Loss Models . . . 6
2.2.1.1. Log-Distance Path Loss Model . . . 6
2.2.1.2. One Slope Model . . . 6
2.2.1.3. Dual Slope Empirical Model . . . 7
2.2.1.4. ITU Model For Indoor Attenuation . . . 8
2.2.2. Picocell Path Loss Models . . . 9
2.2.2.1. Motley-Keenan Model . . . 9
2.2.2.2. Multi Wall and Floor (MWF) Model . . . 10
2.3. Commonly Used Position Estimation Methodologies . . . 11

2.3.1. Trilateration 11
2.3.1.1. Nonlinear Least Squares Method 11
2.3.1.2. Circle Intersections With Clustering 12
2.3.2. WCL 13
2.4. Related Work 15
2.5. Summary of the Chapter and Concluding Remarks 18
3. SIMULATION BASED STUDY OF LOCALIZATION TECHNIQUES . . . 20
3.1. Development of a Simulator for WCL 22
3.2. Evaluation of 3 Beacons Case 22
3.3. Evaluation of 4 Beacons Case 28
3.4. Evaluation of 8 and 16 Beacons Cases 31
3.5. Evaluation of the Trilateration and WCL with Erroneous Channel Model 34
3.6. Comparison of WCL and Trilateration Based on the Implemented Simulations 37
3.7. Summary of the Chapter and Concluding Remarks 38
4. EXPERIMENTAL EVALUATION OF LOCALIZATION METHODS 39
4.1. Development of the Path Loss Measurement System 39
4.1.1. Hardware Design 39
4.1.2. A Brief Explanation of the ZigBee and RSSI Data Reception . . 42
4.1.3. Data Collection 44
4.2. Empirical Channel Model Design 45
4.3. Position Estimation Implementations Based on the Designed Model . . 48
4.4. Summary of the Chapter and Concluding Remarks 49
5. CONCLUSION 50
REFERENCES 51

LIST OF FIGURES

Figure 2.1. Clustered regions among the three trilateration circles. 13

Figure 2.2. Test setup: **x** marks represent the stage data points, the **O** mark represents the tracked object position (instantaneous). 17

Figure 2.3. The K-Nearest Neighbour Match Algorithm. 18

Figure 3.1. Result window of our Trilateration Simulator Tool on Matlab. "+" marker represents the node position, while the "x" markers represent the beacon locations. 21

Figure 3.2. Estimation error vs number of Monte Carlo iterations in Trilateration implementation. 21

Figure 3.3. User interface of our WCL Simulator software. 22

Figure 3.4. Placements of the beacons in three beacons case simulations. . . . 24

Figure 3.5. WCL performance for case 1 displayed in Figure 3.4a. 25

Figure 3.6. WCL performance for case 2 displayed in Figure 3.4b. 25

Figure 3.7. WCL performance for case 3 displayed in Figure 3.4c. 26

Figure 3.8. WCL performance for case 4 displayed in Figure 3.4d. 26

Figure 3.9. WCL performance for case 5 displayed in Figure 3.4e. 27

Figure 3.10. Trilateration performance for all the cases displayed in Figure 3.4. 27

Figure 3.11. Placements of the beacons in four beacons case simulations. 28

Figure 3.12. WCL performance for case 6 displayed in Figure 3.11a. 29

Figure 3.13. WCL performance for case 7 displayed in Figure 3.11b. 29

Figure 3.14. Trilateration performance for the cases displayed in Figure 3.11. . 30

Figure 3.15. Placements of the beacons in eight and 16 beacons cases. 31

Figure 3.16. WCL performance for case 8 displayed in Figure 3.15a. 31

Figure 3.17. WCL performance for case 9 displayed in Figure 3.15b. 32

Figure 3.18. Trilateration performance for case 8 displayed in Figure 3.15a. . . 32

Figure 3.19. Trilateration performance for case 9 displayed in Figure 3.15b. . . 33

Figure 3.20. WCL performance with the ITU Model, $P_f(n)$ parameter of which is provided with 20% error. 34

Figure 3.21. Trilateration performance with the ITU Model, $P_f(n)$ parameter of which is provided with 20% error. 35

Figure 3.22. WCL performance with the ITU Model, $P_f(n)$ parameter of which is provided with 100% error. 35

Figure 3.23. Trilateration performance with the ITU Model, $P_f(n)$ parameter of which is provided with 100% error. 36

Figure 4.1. ZigBee receiver module. 40

Figure 4.2. RSSI transmitter. 40

Figure 4.3. PCB schematic of the RSSI transmitter. 41

Figure 4.4. Circuit diagram of the RSSI transmitter. 41

Figure 4.5. MaxStream XBee. 43

Figure 4.6. Command format for setting the RSSI data provider. 44

Figure 4.7. Path loss vs distance (The blue dots and the red bars represent the average path loss and the variation of the path loss measurements at the related distances, respectively). 45

Figure 4.8. ITU Model path loss estimations vs our measurements (The red curve and the blue plot represent the theoretical path loss estimations of the ITU Model and the measured path loss values, respectively). 46

Figure 4.9. Predictions of our path loss model vs measured path loss values (The red curve and the blue plot represent the theoretical path loss estimations of our model and the real path loss measurements, respectively). 47

Figure 4.10. Position estimations performed by our path loss model with the WCL method. 48

Figure 4.11. Position estimations performed by our path loss model with the Trilateration method. 49

LIST OF TABLES

Table 2.1. Some commonly encountered values of the distance power loss coefficient. 8

Table 2.2. Some commonly encountered values of the floor loss penetration factor. 9

Table 2.3. Examples of penetration losses for the MWF Model. 10

Table 2.4. Mean path loss exponent (η) and standard deviation (σ) for use in the distance-dependent path loss model based on the measurements at 914MHz carrier frequency, according to the placements of the transmitter and the receiver. 19

LIST OF ACRONYMS/ABBREVIATIONS

CL	Centroid Localization
ITU	International Telecommunications Union
LoS	Line of Sight
PAN	Personal Area Network
PWM	Pulse Width Modulation
RSSI	Received Signal Strength Indicator
UART	Universal Asynchronous Receiver/Transmitter
WCL	Weighted Centroid Localization

1. INTRODUCTION

Position estimation in wireless sensor networks gets highly important since many applications require positional data related to the measurements with minimal error. Most of the position estimation methods are based on distance estimation, which requires successful channel modelling. There are several channel models previously developed and published, but each transmission media has its specific channel characteristics, such that a position estimation implementation based on present channel models may fail. This thesis is focused on designing an indoor position estimation system based on an indoor radio channel model that is also developed herein.

Using a channel model designed specifically for the indoor area, where the position estimation is to be implemented, results successful estimates with minimal error. The indoor channel model is developed empirically by applying Least Squares Method on the redundant RSSI data collected from different distances to the transmitter antenna. Distance estimation, which constitutes the basis of position estimation, is performed using the developed indoor channel model. Since the RSSI data is collected in an industrial area, the developed channel model can be said to be an empirical indoor radio propagation channel model for industrial areas.

1.1. Commonly Used Distance Estimation Methodologies

A brief overview of the commonly used distance estimation methodologies is presented below.

1.1.1. RSSI

RSSI is the information related to the received power on the antenna during the related data packet reception. It is possible to use RSSI based position estimation algorithms in media where LoS data transfer is available [1]. The RSSI value related to any received data packet is available at the physical layer in the IEEE 802.15.4

network. Using the RSSI values, relative distance to any node can be estimated based on a channel model, enabling the design of position estimation algorithms which use a couple of estimated relative distances to the node in question.

1.1.2. Uplink-Time Difference of Arrival (U-TDoA)

The difference between the arrival times of signals sent from different base stations is used as the distance data of the device to the base stations. Using the collected time difference data, the distance from base station to the device could be easily estimated, such that with the estimated distances, localization of the device can be easily implemented using position estimation algorithms.

1.1.3. Time of Arrival (ToA)

The Time of Arrival methodology uses the absolute time of arrival at a base station rather than the arrival time difference between two stations. Using the absolute arrival time of the received data packet, the distance can be calculated considering the signal travelling with the speed of light (300,000 kilometers per second). For instance, a distance estimation procedure can be implemented as follows: A node sends a query message to the other, and then starts a timer and counts until it receives a response to the query. Then it uses the integer counted by the timer as the data representing the distance to the other node.

Identifying the exact coordinates of sensor nodes (also called unknown nodes or unknowns) requires measuring distances from a sufficient number of reference points to the node in question by using one of the distance estimation methodologies as explained above. Time measurement based distance estimation methods may tend to synchronization problems of involved devices as well as necessity of high mathematical effort to calculate the position. Although measuring the received signal strength offers a possibility to determine distance with minimal effort, still it has several deficiencies such as causing unreliability, requiring redundant measurements and calculations.

1.2. The Organization of the Thesis

Chapter 2 presents a review of the relevant literature on factors causing path loss and indoor channel path loss models. Following the path loss models, we introduce the two basic position estimation methods, Trilateration and WCL.

In Chapter 3, we run simulations to study both Trilateration and WCL with simulator tools we have designed. We run simulations in order to examine the estimation error rates of the methods versus varying crucial parameters of the models.

In Chapter 4, we introduce our indoor position estimation system including design steps and performance testings. Initially, our RSSI measurement system design and data collection procedures are presented. Then, our indoor channel model design based on the collected RSSI measurements is introduced, and position estimation implementations based on our channel model with both of the told position estimation methods (Trilateration and WCL) are shown.

2. REVIEW OF INDOOR RADIO CHANNEL MODELS AND POSITIONING METHODS

In this chapter; path loss definition, indoor channel models, popular position estimation methodologies and previous studies related to these topics are reviewed, since such an understanding of path loss and channel modelling is crucial for the design procedures of an indoor position estimation system.

Path loss is the power density reduction of a radio signal as it propagates through space, and mathematically, it can be explained as the difference (in dB) between the transmitted signal power and the received signal power, as in Equation 2.1.

$$L = 10 \cdot \log(P_{TX}/P_{RX}) \tag{2.1}$$

where L is the path loss in dB, P_{TX} is the transmission power of the sender in Watts, and P_{RX} is the remaining power of a wave at the receiver in Watts.

Path loss is the major component in the design and analysis of the link budget of a radio communication system. Path loss is also affected by environmental factors like obstacles located on the line of sight of the signal transmission, propagation medium and especially the distance between the transmitter and the receiver, and also the height and location of antennas.

2.1. Factors Causing Path Loss

Free space loss, fading, multipath and refraction are the leading factors causing path loss. Brief information about the complications in question is presented below.

2.1.1. Free Space Loss

Radio signals disperse with distance, so when the distance between the receiver and the transmitter antennas increase, less signal power is induced at the receiver side. Even if no other impairments are present, the signal attenuates over distance since it is spread over a larger area during transmission.

2.1.2. Fading

Fading is the variability of the power of a wireless signal depending on the environmental effects such as changing atmospheric conditions for fixed environments, and changing numbers and locations of the obstacles blocking wireless transmission for the mobile media.

2.1.3. Multipath

Multipath problem is the arrival of a radio signal to the destination antenna by two or more paths. The problem arises from the direct and reflected signals that are often opposite in phase. These signals may cancel out each other causing data loss at the receiver antenna. Multipath problem generally occurs in environments where metallic surfaces are present. There are three types of the Multipath problem which are Reflection, Diffraction and Scattering. Reflection occurs when the radio signal reaches an object which is much larger than the wavelength of the signal such as buildings and walls, while Diffraction takes place if the wavelength of the signal is smaller than the obstacle sizes. Besides, Scattering is originated from the obstacles that are small with respect to the wavelength and the number of obstacles that are large per unit volume, such as sand or rough surfaces.

2.1.4. Refraction

Refraction is the change in direction of an electromagnetic wave due to the changes in the propagation velocity of the medium through which the signal is be-

ing transmitted, and only a fraction or no part of the LoS wave reaches the receiver.

2.2. Commonly Used Indoor Channel Path Loss Models

Indoor channel path loss models are categorized as Microcell path loss models and Picocell path loss models, according to the coverage area.

2.2.1. Microcell Path Loss Models

A Microcell is the name of the cells in a mobile network fed by low power cellular base stations, covering a limited area. Operating area examples for a Microcell can be listed as hotels, malls, or transportation hubs. A Microcell controls the output power to limit its coverage area. Radius of a typical coverage area of a Microcell is less than 2 km, while standard base stations are able to communicate through distances up to 35 km.

2.2.1.1. Log-Distance Path Loss Model. The Log-Distance Path Loss Model is an indoor radio propagation model which estimates the attenuation of a radio signal that occurs while the signal travels in a closed area. The model is formally expressed in Equation 2.2 [2].

$$L(d) = L(d_0) + 10 \cdot \eta \cdot log(d/d_0) + X_g \tag{2.2}$$

where $L(d)$ is the total path loss measured in dB at distance d, $L(d_0)$ is the path loss at the reference distance d_0 which is generally taken as 1m, η is the path loss exponent, and X_g is a zero mean Gaussian random variable, modelling the shadowing effect on the received signal power.

2.2.1.2. One Slope Model. One slope path loss model sets the value of the power decay index based on experimental data, hence it can be said to be a semi-empirical model.

The received signal power is modelled as in Equation 2.3 [2]:

$$L(d) = K + 10 \cdot \eta \cdot log(d/d_0) \tag{2.3}$$

where K is the constant which depends on the antenna characteristics and the average channel attenuation, d_0 is the reference distance for the antenna, and η is the power decay index. The value of η depends on the propagation environment. For complex environments it is more practical to obtain the power decay index using a curve fitting method for minimum mean square error (MMSE), fitting to the empirical measurements.

2.2.1.3. Dual Slope Empirical Model. Dual slope model is another indoor path loss model which is designed to be more accurate when compared to the one slope model [2]. It is said to be more accurate since two separate path loss exponents are used to characterize the signal propagation. The breakpoint is a few hundred meters (i.e. the secondary path loss exponent is taken in charge when the distance is greater than a predefined threshold value, which is a few hundred meters). In the dual slope empirical model, the loss is expressed by [2]

$$L(d) = \begin{cases} 10 \cdot \eta_1 \cdot \log(d) + L(1), & \text{if } d \leq d_b \\ 10 \cdot \eta_2 \cdot \log(d/d_b) + 10 \cdot \eta_1 \cdot \log(d_b) + L(1), & \text{otherwise} \end{cases} \tag{2.4}$$

where $L(1)$ is the reference path loss at $d = 1m$, d_b is the breakpoint distance, η_1 is the path loss exponent for $d \leq d_b$, and η_2 is the path loss exponent for $d > d_b$.

Equation 2.4 can be modified as in Equation 2.5 to avoid sharp transitions:

$$L(d) = L_0 + 10 \cdot \eta_1 \cdot \log(d) + 10 \cdot (\eta_2 - \eta_1) \cdot \log(1 + d/d_b) \tag{2.5}$$

The parameters η_1 and η_2 are usually assigned as 2 and 4, respectively, but these values may vary depending on the environment in which the signal transmission is

being performed.

2.2.1.4. ITU Model For Indoor Attenuation. The ITU Indoor Propagation Model, also known as ITU Model for Indoor Attenuation, is a radio propagation model that is used to estimate the path loss inside a closed area delimited by walls. As being a suitable indoor channel model, the ITU Indoor Propagation Model approximates the total path loss that an indoor link may experience. While the model is applicable only to the indoor environments, generally it uses the lower microwave bands around 2.4 GHz. However, the model is suitable to be applied to a much wider range. Mathematical formulation of this model is given by [3]

$$PL_{ITU}(d) = 20 \cdot \log(f) + N \cdot \log(d) + P_f(n) - 28 \tag{2.6}$$

where $PL_{ITU}(d)$ is the total path loss in dB, f is the data transmission frequency in megahertz (MHz), d is the distance between the receiver and the transmitter antennas in meters (m), N is the distance power loss coefficient, n is the number of floors or walls to be penetrated between the transmitter and the receiver, and $P_f(n)$ is the floor loss penetration factor.

The distance power loss coefficient, N, is the empirically determined quantity which expresses the loss of signal power with distance. Some commonly encountered values for the distance power loss coefficient are given in Table 2.1 [3].

Table 2.1. Some commonly encountered values of the distance power loss coefficient.

Frequency Band	**Residential**	**Office**	**Commercial**
900MHz	N/A	33	20
1.2GHz	N/A	32	22

The other empirically defined parameter of the model is the floor loss penetration factor ($P_f(n)$). It is dependent on the number of floors or walls, to be penetrated for the

radio waves during the wireless communication. Some commonly encountered values are given in Table 2.2 [3].

Table 2.2. Some commonly encountered values of the floor loss penetration factor.

Frequency	**Floors**	**Residential**	**Office**	**Commercial**
900MHz	1	N/A	9	N/A
900MHz	2	N/A	19	N/A
900MHz	3	N/A	24	N/A
1.8GHz	n	4n	15+4(n-1)	6 + 3(n-1)
2.0GHz	n	4n	15+4(n-1)	6 + 3(n-1)
5.2GHz	1	N/A	16	N/A

2.2.2. Picocell Path Loss Models

Picocell is the name of small cellular base stations covering a small area, such as in-building, or in-aircraft. Picocells are generally used in indoor areas to extend the coverage, or increase network capacity where outdoor signals do not reach well. Picocells provide more coverage and capacity in areas where it is difficult or expensive to reach using the more traditional microcell approach.

2.2.2.1. Motley-Keenan Model. This model is developed by Motley and Keenan, considering all the penetrated walls and floors by individual penetration losses according to their thickness and materials [4]. The model assumes that the same type of walls and floors (in terms of thicknesses and materials) contribute a constant loss, no matter other walls or floors have been penetrated before [5]. The mathematical representation of the model is given by

$$L(d) = L(0) + 10 \cdot \eta \cdot \log(d) + \sum_{i=1}^{N} k_i \cdot L_{wi} + \sum_{j=1}^{M} k_j \cdot L_{fj} \tag{2.7}$$

where N is the total number of the wall types, k_i is the number of walls of type i, L_{wi} is the penetration loss due to the type i wall, M is the total number of the floor types, k_j is the number of floors of type j, and L_{fj} is the penetration loss due to the type j floor.

2.2.2.2. Multi Wall and Floor (MWF) Model. The Multi Wall and Floor Model can be said to be an enhanced version of the Motley-Keenan Model. It takes into account the decreasing penetration losses of walls and floors of the same material as their number increases, rather than assuming that attenuation does not depend on the number of walls or floors penetrated before. Mathematical expression of the model is given by

$$L(d) = L(0) + 10 \cdot \eta \cdot \log(d) + \sum_{i=1}^{I} \sum_{k=1}^{K_{wi}} L_{wik} + \sum_{j=1}^{J} \sum_{k=1}^{K_{fj}} L_{fjk} \tag{2.8}$$

where L_{wik} is the attenuation due to the kth traversed wall type i, L_{fjk} is the attenuation due to the kth traversed floor type j, I is the number of walls, K_{wi} is the number of traversed walls of type i, J is the number of floors, and K_{fj} is the number of traversed floors of type j.

Table 2.3 shows some measured attenuation values due to penetration.

Table 2.3. Examples of penetration losses for the MWF Model.

Wall Material	**Thickness**	**1st penetration**	**2nd penetration**
Concerete	10 cm	16 dB	14 dB
Concerete	20 cm	29 dB	24 dB
M1	T cm	35 dB	29 dB
M2	T cm	34 dB	26 dB

2.3. Commonly Used Position Estimation Methodologies

In this part, commonly used position estimation algorithms, the Trilateration and WCL, are reviewed.

2.3.1. Trilateration

We now briefly review the Trilateration method based on the work of [6]. Consider a node N with an unknown location (n_x, n_y) and three beacons A, B and C, known as the positions (a_x, a_y), (b_x, b_y) and (c_x, c_y), respectively. The trilateration problem is to compute the coordinates of the node N, given the distances d_a, d_b and d_c, from the node to the beacons A, B and C, respectively. Since the distances to the beacons are typically measured with errors, it is needed to follow one of the two ways of solving the trilateration problem which are nonlinear least squares and circle intersections with clustering.

2.3.1.1. Nonlinear Least Squares Method. Using the estimated distances from the node to the three beacons, we derive the following system of equations:

$$(n_x - a_x)^2 + (n_y - a_y)^2 - d_a^2 = 0 \tag{2.9}$$

$$(n_x - b_x)^2 + (n_y - b_y)^2 - d_b^2 = 0 \tag{2.10}$$

$$(n_x - c_x)^2 + (n_y - c_y)^2 - d_c^2 = 0 \tag{2.11}$$

Due to the errors in path loss measurements causing distance estimation errors, right hand sides of Equations 2.9 - 2.11 are nonzero, thus the system does not have a solution. Rewriting the expressions as in Equations 2.12 - 2.14, where the zeroes on the right

hand sides have been replaced by nonzero residuals:

$$(n_x - a_x)^2 + (n_y - a_y)^2 - d_a^2 = a_\delta \tag{2.12}$$

$$(n_x - b_x)^2 + (n_y - b_y)^2 - d_b^2 = b_\delta \tag{2.13}$$

$$(n_x - c_x)^2 + (n_y - c_y)^2 - d_c^2 = c_\delta \tag{2.14}$$

The least squares solution is the unique solution (n_x, n_y) that minimizes the sum of the squares of the residuals $({a_\delta}^2 + {b_\delta}^2 + {c_\delta}^2)$. The system of equations is nonlinear due to the squared terms. Thus, a nonlinear least squares algorithm is needed to calculate the solution. An efficient way is to start from an initial guess at the solution and then iteratively modify the candidate solution to reach the minimum squared residuals sum.

2.3.1.2. Circle Intersections With Clustering. Consider the circles of radii d_a, d_b and d_c around points A, B and C, respectively. Since the circles' centers and radii, derived from path loss measurements together with the considered channel model, are obtained with measurement errors, the circles will not intersect at a single point and probably overlap in a small region, where the unknown node N is located inside. If the measurement errors are not extremely high, then each pair of circles yields two intersection points. Three of these points are clustered closely together, while the others are located far from this group. The node N is located in the middle of this cluster as shown in Figure 2.1 [6].

A practical way of finding the cluster is as follows: The distance between each pair of circle intersection points is calculated. The closest two intersection points are picked to be the initial cluster and then the centroid of the cluster is calculated. The abscissa of the centroid is the average of the abscissas of the points in the cluster; and similarly the centroid's ordinate is the average of the ordinates of the points in

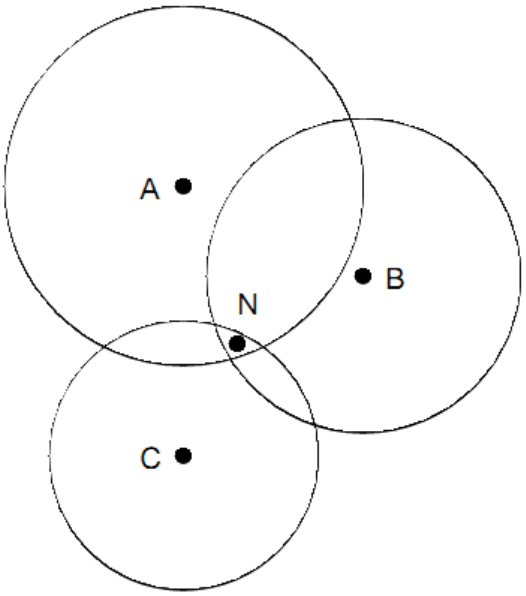

Figure 2.1. Clustered regions among the three trilateration circles.

the cluster. Next, the circle intersection point that is closest to the cluster centroid is found, and this intersection point is added to the cluster and cluster centroid is recomputed. The result centroid is the estimated position of the node N.

2.3.2. WCL

We now review the position estimation method WCL based on the study of [7]. Consider a sensor network with a total number of k nodes consisting of n sensor nodes and m beacons ($m << n$). Beacons are assumed to include improved position detection systems like GPS, so they are able to determine their own coordinates. Therefore, the locations of the beacons are assumed to be the true coordinates. The nodes initially do not know their own locations. The nodes and beacons are deployed on an area with uniform distribution. The CL algorithm, which is previously published by [8], is simply based on the nodes' averaging the received coordinates broadcast by the surrounding beacons. Each beacon broadcasts its coordinates in a limited range usually covering only a small portion of the area where the nodes are distributed. The mathematical

representation of the algorithm is given by

$$P_i^{(CL)}(x,y) = (1/n)\sum_{j=1}^{n} B_j(x,y) \tag{2.15}$$

where $P_i^{(CL)}(x,y)$ is the estimated coordinates of the ith node, $B_j(x,y)$ is the exact coordinates of the jth beacon, and n is the number of beacons, coordinates of which are received by the ith node.

The disadvantage of the CL approach is that two or even more nodes located completely in different positions may be covered by exactly the same beacons (e.g. 3^{rd}, 7^{th} and 13^{th} beacons among others). In this case all these nodes will estimate the same coordinates as their positions. Hence, plenty of beacons with minimum transmission ranges should be placed, in order for the nodes to estimate their positions with minimum collision. Furthermore, $B_n!$ different positions can be generated using this method, where B_n is the number of beacons.

The WCL, proposed by [7], is an extension of the CL algorithm. In WCL, every position data received by a node is added to the sum after being multiplied by a weight coefficient between the node and the beacon. The same procedure is implemented for each of the beacons covering the subject node. Once the sum is obtained, then it is divided by the sum of all the weight coefficients between the subject node and the communicated beacons. The mathematical expression of the method is given by

$$P_i^{(WCL)}(x,y) = \frac{\sum_{j=1}^{n}(\omega_{ij} \cdot B_j(x,y))}{\sum_{j=1}^{n}\omega_{ij}} \tag{2.16}$$

where $P_i^{(WCL)}(x,y)$ is the estimated coordinates of the ith node, $B_j(x,y)$ is the exact coordinates of the jth beacon, and ω_{ij} is the weight coefficient between the ith node and the jth beacon.

Note that equating $\omega_{ij} = 1$ for all i, j; we get the simple CL algorithm in Equation 2.15. Considering a concentric wave expansion with a linear characteristic of the

receiver and a uniform density of the beacons, researchers form the weight coefficients as [7]:

$$\omega_{ij} = \frac{1}{(d_{ij})^g} \tag{2.17}$$

where ω_{ij} is the weight coefficient between the ith node and the jth beacon, d_{ij} is the distance between the ith node and the jth beacon, and g is the weighting degree.

Increasing the weighting degree, decreases the effect of the far away beacons marginally, but increasing it too much will make a node to estimate its coordinates nearly the same with the nearest beacon, increasing the error. Hence the weighting degree has to be optimized.

2.4. Related Work

Researchers preferred RSSI technique in position estimation, methodology of whom is discussed in [7]. Measuring the received signal strength provides researchers to achieve distance determination with minimal effort. RSS logic is based on the fact that the output power of the transmitting device (P_{TX}) directly affects the receiving power at the receiving side (P_{RX}). Based on Friis' free space transmission equation expressed in [7], free space path loss model can be formed as

$$L(d) = -10 \cdot \log(G_{TX} \cdot G_{RX} \cdot (\lambda/4\pi d)^2) \tag{2.18}$$

where G_{TX} is the gain of the transmitter, G_{RX} is the gain of the receiver, λ is the wave length, and d is the distance between sender and the receiver.

RSSI can be generated in dB using a reference signal strength P_{Ref} value (usually taken as $1mW$), as in Equation 2.19:

$$RSSI = 10 \cdot \log\left(P_{RX}/P_{Ref}\right) \tag{2.19}$$

where P_{RX} is the remaining power of a wave at the receiver in Watts.

Received signal strength values are not reliable enough since radio signals are exposed to many manipulating effects such as; reflections on metallic objects, diffraction at edges, refraction by media with different propagation velocity, polarization of electro-magnetic fields, and inapplicable receiving circuits [7].

Another method which can be used to estimate a distance from a node to reference points is the Link Quality Indication (LQI) which is provided by the ZigBee Protocol as a quality indicator of a received packet. LQI represents a number of required transmission attempts to receive a radio packet correctly at the receiver. The scenario on which Ralf Grossman worked consists of a ZigBee device, which is a reference beacon continuously transmitting data, and a listener ZigBee device recording the LQI values of the packets [7]. Distance between these two nodes is tuned from 0 meters to 40 meters. After the procedure, its seen that the changes in the LQI values are just as expected so that the values increase as the nodes get closer and decrease as they are taken far from each other.

Another related research deals with the problem of learning real time coordinates of nodes from a single control point [9]. The researchers studied on two different methods. The first one is based on ToA (Time of Arrival) approach such that a node sends a query and the other responds as soon as it receives the query message. The one has sent the query message measures the time passed until it receives the response of the other one. But since the variance of the data package processing time is much longer than changes in the data arrival periods depending on the distance between the two nodes; this method is not that much reliable. The second method proposed by [9] as a solution to this problem is as follows: A ZigBee module operating in router mode (see Section 4.1.2) broadcasts the unique ID of the device, coordinates of which is to be determined, and then starts a timer immediately. Once the unique ID is broadcast, only the node, unique ID of which matches with the broadcast one, sends an ultrasonic wave as a response. The router stops its timer when it receives the ultrasonic wave. Since transmission speed of the ultrasonic waves is very slow with respect to the RF

signal transmission speed, and variances in the periods of the embedded processes are negligible when compared to the speed of ultrasonic waves, distance estimation is much more reliable in this method.

In the work of [10], which is another study on RSSI based position estimation, the researchers applied the method named K-Nearest Neighbour Match Algorithm on a test setup represented in Figure 2.2.

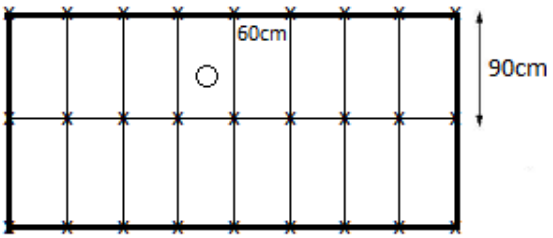

Figure 2.2. Test setup: **x** marks represent the stage data points, the **O** mark represents the tracked object position (instantaneous).

During the experimentation; for each of the map building stage data points (beacons), approximately 60000 samples of RSSI data are collected for 2 minutes for two different mote orientations: 180^o and -180^o. For each orientation, mean RSSI data was computed and stored in the data set γ, along with the point coordinates. Data is collected separately for the two different orientations to observe the effect of mote orientation on the estimation error. The algorithm is given below [10]:

The authors of [10] examined the estimation error by varying the parameter k, which is the number of candidate neighbors chosen for interpolation. They observed that as the parameter k is increased, the estimation error decreases until it reaches an absolute minimum, and then increases rapidly.

As an indoor radio propagation example, [11] presents the authors' experiments in path loss measurements in a multi floored building. Equation 2.20 proposed by the researchers is intended to be used in path loss calculation in a multi floored building.

Find k-Nearest;
$N = sizeof(\gamma)$;
for $i = 1$ to N **do**
  $Distance[i] = ||RSSI.value - \gamma[i].value||$;
  Sort Ascending($Distance$);
  $k - Nearest = Distance[1 : k]$;
  $Location_{Estimated} = mean(k - Nearest)$;
end for

Figure 2.3. The K-Nearest Neighbour Match Algorithm.

The equation is similar to the generic path loss expression but emphasizes that the mean path loss exponent (η) is a function of the number of floors between the transmitter and the receiver. The values of $\eta(multifloor)$ are given in Table 2.4, which are the mean of the path loss exponent values measured after several iterations and from different locations [11].

$$L(d) = L(d_0) + 10 \cdot \eta(multifloor) \cdot \log(d/d_0) \tag{2.20}$$

where $L(d)$ is the total path loss at distance d, $L(d_0)$ is path loss at the reference distance d_0, and $\eta(multifloor)$ is the experimentally obtained path loss exponent depending on the number of floors to be penetrated by the radio signal.

2.5. Summary of the Chapter and Concluding Remarks

In this chapter, factors causing path loss and commonly used indoor path loss models are reviewed. Since radio signals are subject to be distorted and attenuated due to a combination of the reviewed factors causing path loss, determining the total path loss by an analytic way is not an easy task. In addition to an overview of the path loss models, the most popular position estimation methods, Trilateration and the WCL, are also reviewed.

Table 2.4. Mean path loss exponent (η) and standard deviation (σ) for use in the distance-dependent path loss model based on the measurements at 914MHz carrier frequency, according to the placements of the transmitter and the receiver.

	η	σ **(dB)**	**number of locations**
Same floor	2,76	12,9	501
Through 1 floor	4,19	5,1	73
Through 2 floors	5,04	6,5	30
Through 3 floors	5,22	6,7	30
All locations	3,14	16,3	634

3. SIMULATION BASED STUDY OF LOCALIZATION TECHNIQUES

As a preliminary work of indoor position estimation system design, we tested the most common two position estimation methodologies: WCL and Trilateration. There are two important parameters for both methods to perform successful estimations, which are the number and the position of the beacons. Besides, there is an additional crucial parameter for the WCL methodology which is the weighting degree. We developed a software program (WCL Simulator) in C Sharp.NET to simulate the WCL method, and a Matlab tool to simulate the Trilateration (see Figure 3.1). We tested both of the methods with various beacon placements, with the aim of optimizing the position estimation setup. We implemented the algorithms for all the possible node locations on the 2-D field model of 400 units width and 600 units length, setting the weighting degree for WCL to 2.77, which is the derived path loss exponent in the empirical channel model development (see Section 4.2). We run both methods by applying the same random noise vector on the distance values to model the unreliability of RSSI data.

We used the circle intersections with clustering method in the Trilateration implementations. We run the Trilateration algorithm by performing Monte Carlo simulations with 400 iterations, which can be said to be a reasonable number considering the simulation results displayed in Figure 3.2.

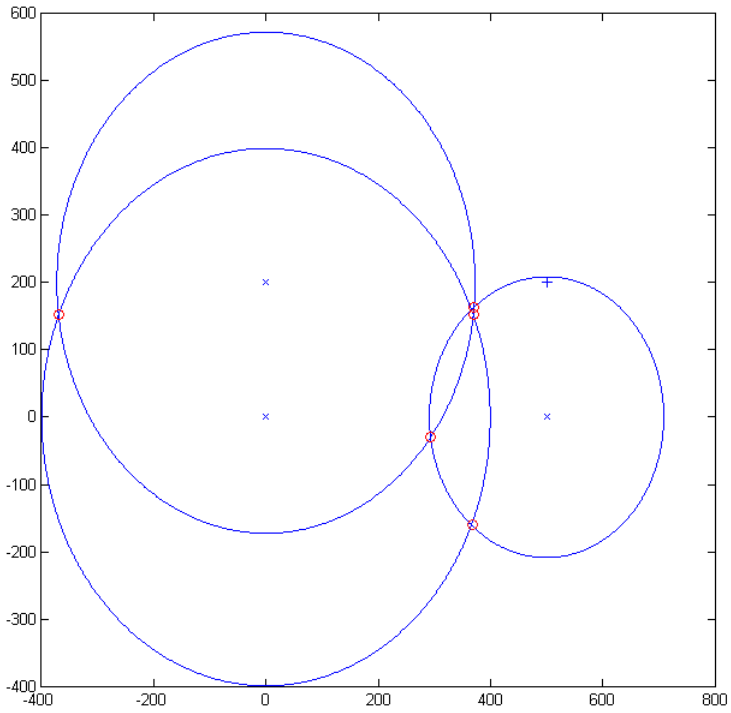

Figure 3.1. Result window of our Trilateration Simulator Tool on Matlab. "+" marker represents the node position, while the "x" markers represent the beacon locations.

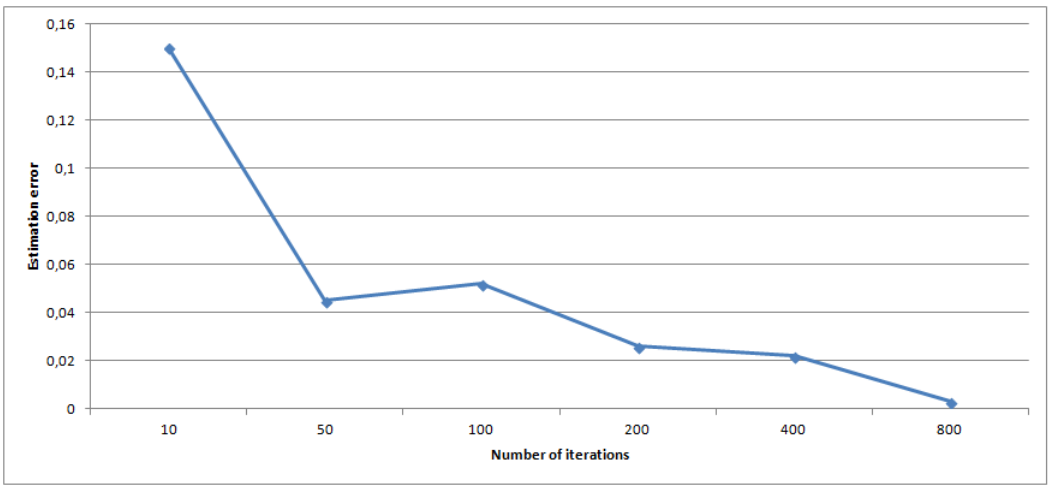

Figure 3.2. Estimation error vs number of Monte Carlo iterations in Trilateration implementation.

3.1. Development of a Simulator for WCL

The WCL Simulator has a graphical user interface (see Figure 3.3), on which the simulation test setup is represented including the beacon locations and, the actual and estimated locations of the nodes. The red and the black dots on the test setup represent the beacon locations and the actual node locations, respectively. The green dots represent the location estimation results of the algorithm when it is run with noisy distance data (i.e. random noise is applied on the distances between the nodes and beacons). The pink dots represent the estimated node locations when the WCL algorithm is run in the no noise case. After the user locates the beacons and nodes, WCL Simulator implements the WCL algorithm and lists the error percentage versus the varying weighting degree.

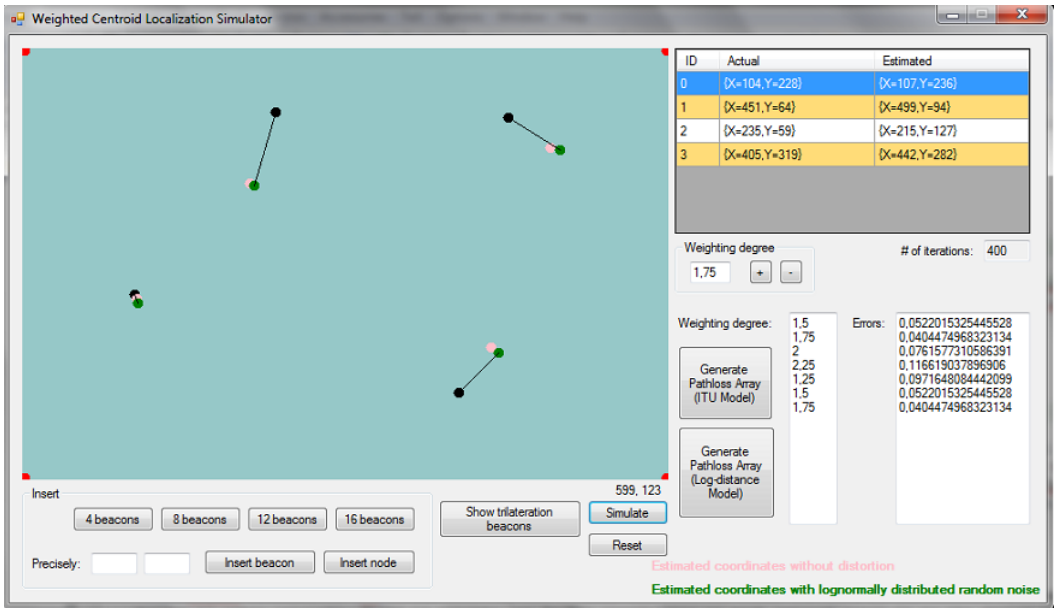

Figure 3.3. User interface of our WCL Simulator software.

3.2. Evaluation of 3 Beacons Case

In this section we evaluate the performance of the two algorithms for the following 5 configurations as shown in Figure 3.4. Figures 3.4a - 3.4e represent the beacon placements in each configuration. For instance, let (x, y) be any location on the 2-D

simulation field, then beacons are located at $(2, 2)$, $(2, 398)$ and $(598, 398)$ on the 2-D simulation field of 400 units width and 600 units length in the beacon placement case 1 as displayed in Figure 3.4a. Similarly, beacon locations are $(2, 398)$, $(300, 2)$ and $(598, 398)$ in case 2 as displayed in Figure 3.4b, $(2, 2)$, $(2, 398)$ and $(598, 200)$ in case 3 as displayed in Figure 3.4c, $(2, 200)$, $(300, 398)$ and $(598, 200)$ in case 4 as displayed in Figure 3.4d, $(300, 2)$, $(300, 398)$ and $(598, 200)$ in case 5 as displayed in Figure 3.4e. With these beacon placement configurations we aim to examine the performances of the Trilateration and WCL for all the significant beacon placement variations possible with 3 beacons on a rectangular 2-D field. We simulate the algorithms for all possible node locations on the simulation field. Simulation results are shown in Figures 3.5 - 3.10.

In the simulation results shown in Figures 3.5 - 3.9 it is seen that estimation error of WCL increases excessively as the unknown node position gets out of the borders set by the beacons. Besides, mean errors of WCL estimations in cases 1, 2, 3, 4 and 5 are found as 25.7%, 17.3%, 19.1%, 25.2%, and 22.3%, respectively. Thus, beacon placements in case 2 (see Figure 3.4b) can be said to be the optimal beacon deployment formation for a WCL based position estimation system with three beacons.

On the other hand, it is seen that the performance of Trilateration stays constant in all the five deployment formations in question. The estimation errors of Trilateration for the three beacons cases displayed in Figure 3.10 is only due to the random noise matrix applied to the distance data between the node and the beacons, duplicate of which is also applied in WCL estimations.

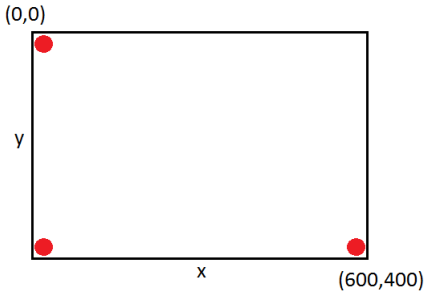

(a) Beacon placement case 1.

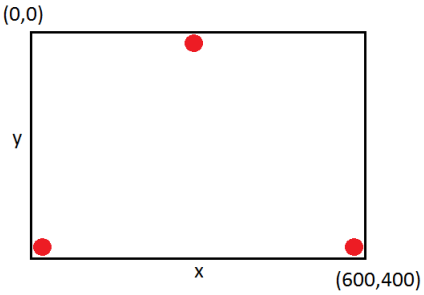

(b) Beacon placement case 2.

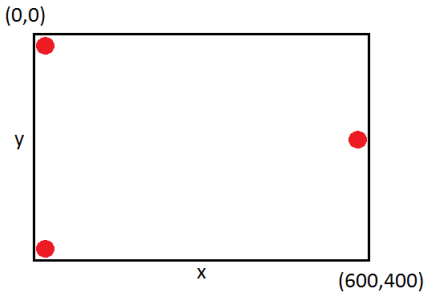

(c) Beacon placement case 3.

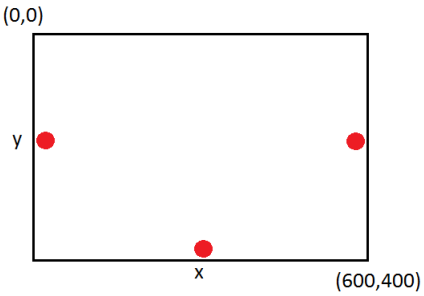

(d) Beacon placement case 4.

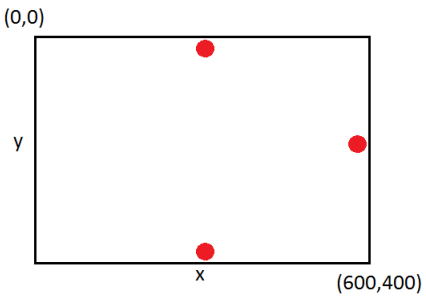

(e) Beacon placement case 5.

Figure 3.4. Placements of the beacons in three beacons case simulations.

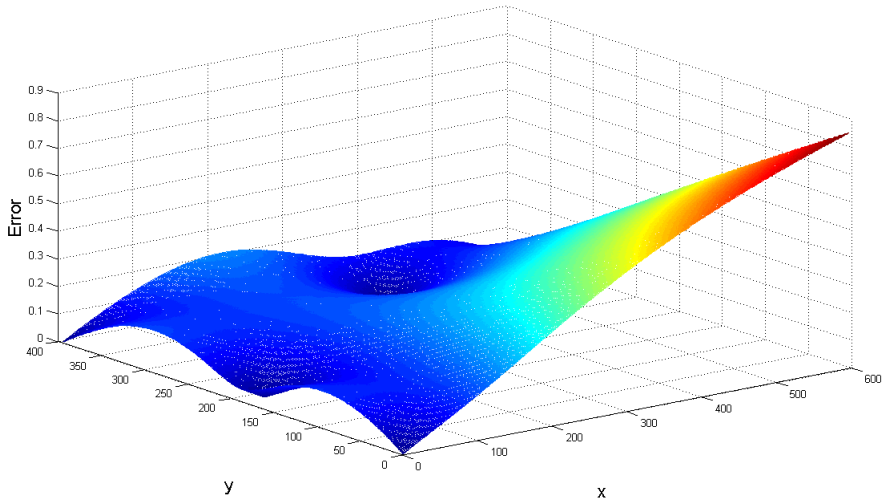

Figure 3.5. WCL performance for case 1 displayed in Figure 3.4a.

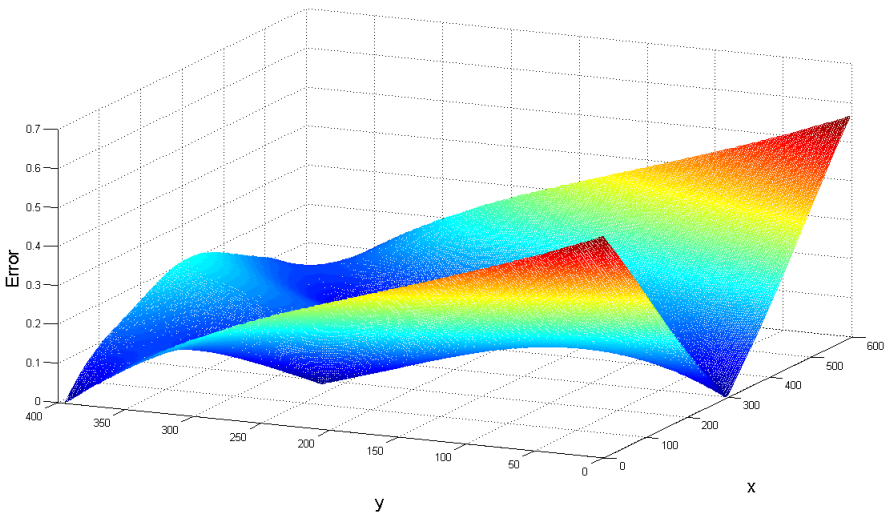

Figure 3.6. WCL performance for case 2 displayed in Figure 3.4b.

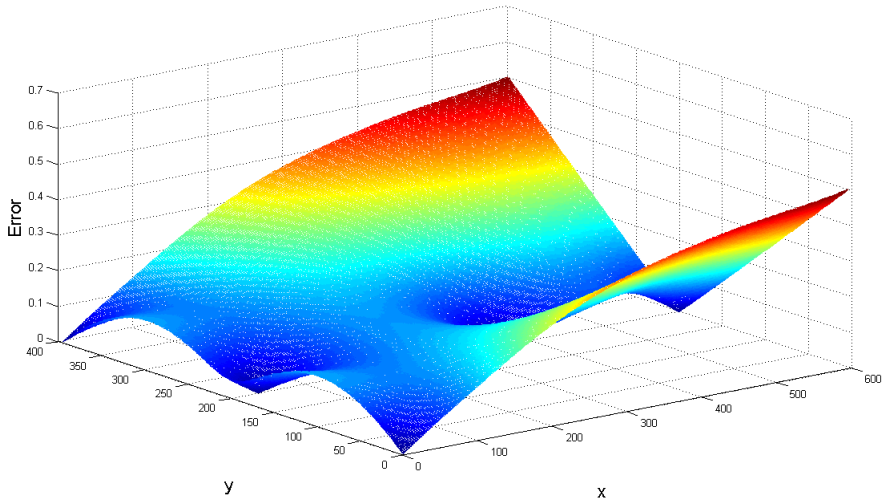

Figure 3.7. WCL performance for case 3 displayed in Figure 3.4c.

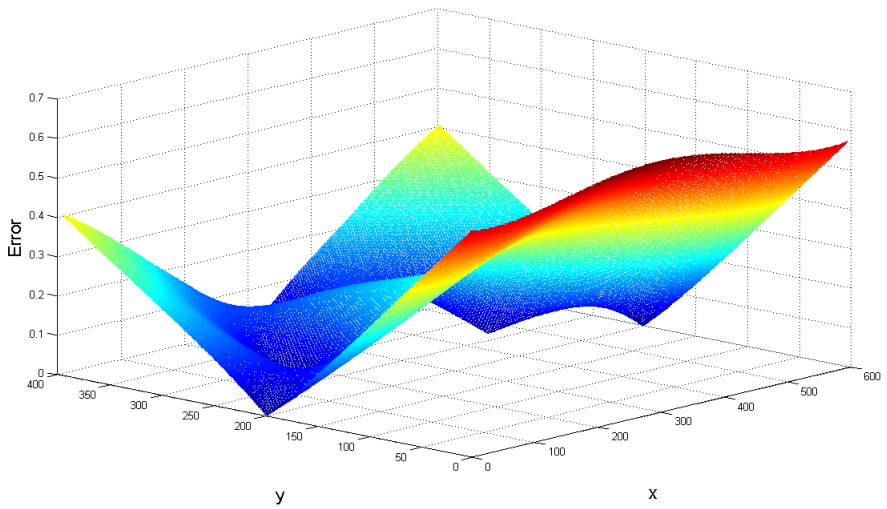

Figure 3.8. WCL performance for case 4 displayed in Figure 3.4d.

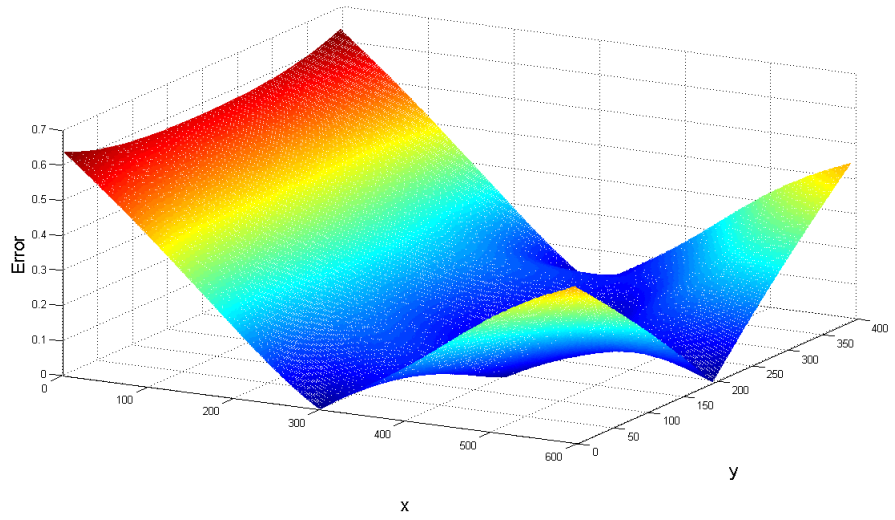

Figure 3.9. WCL performance for case 5 displayed in Figure 3.4e.

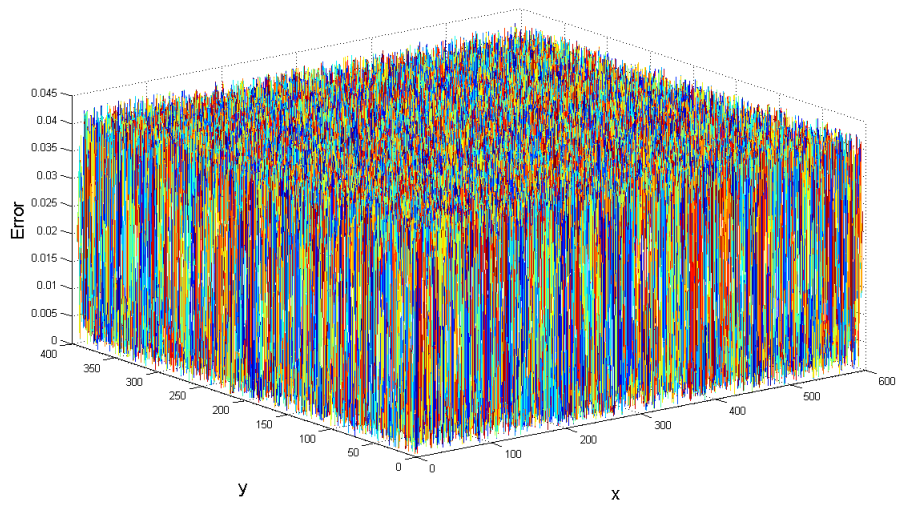

Figure 3.10. Trilateration performance for all the cases displayed in Figure 3.4.

3.3. Evaluation of 4 Beacons Case

In this section, we evaluate the performance of the Trilateration and WCL algorithms for 2 different beacon placement configurations with four beacons as shown in Figure 3.11. Beacon locations are $(2, 2)$, $(2, 398)$, $(598, 2)$ and $(598, 398)$ in beacon placement case 6 displayed in Figure 3.11a, and $(2, 200)$, $(300, 2)$, $(300, 398)$ and $(598, 200)$ in beacon placement case 7 displayed in Figure 3.11b.

The Trilateration algorithm is modified such that the algorithm takes the average of the results obtained from the four different combinations built by different three beacons sets. This modification is set active for all the Trilateration simulations for the cases where the number of beacons is greater than 3. Results of the four beacons case simulations are shown in Figures 3.12 - 3.14.

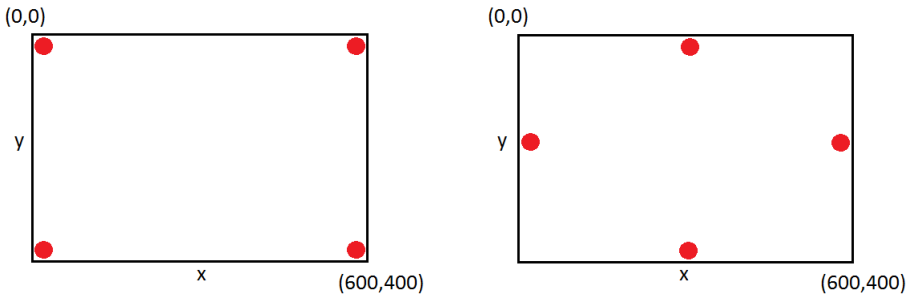

(a) Beacon placement case 6. (b) Beacon placement case 7.

Figure 3.11. Placements of the beacons in four beacons case simulations.

Simulation results displayed in Figure 3.12 show that performance of WCL decreases as the node gets closer to the centroid of two beacons located on a common edge of the field. On the other hand, considering the error distribution displayed in Figure 3.13 it is again seen that estimation error increases as the node gets out of the borders set by the beacons. Moreover mean errors of WCL in beacon placement cases 6 and 7 are found as 16.6% and 14%. Thus, beacon deployment formation displayed in Figure 3.11b can be said to be the appropriate one for a WCL based position estimation system with four beacons. Besides, Trilateration performance again stays constant independently from the beacon placements. But it is worth to note that estimation

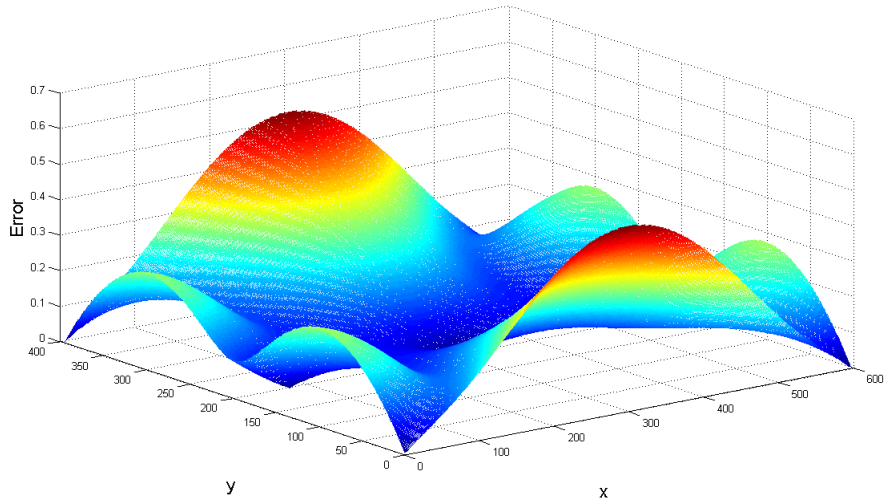

Figure 3.12. WCL performance for case 6 displayed in Figure 3.11a.

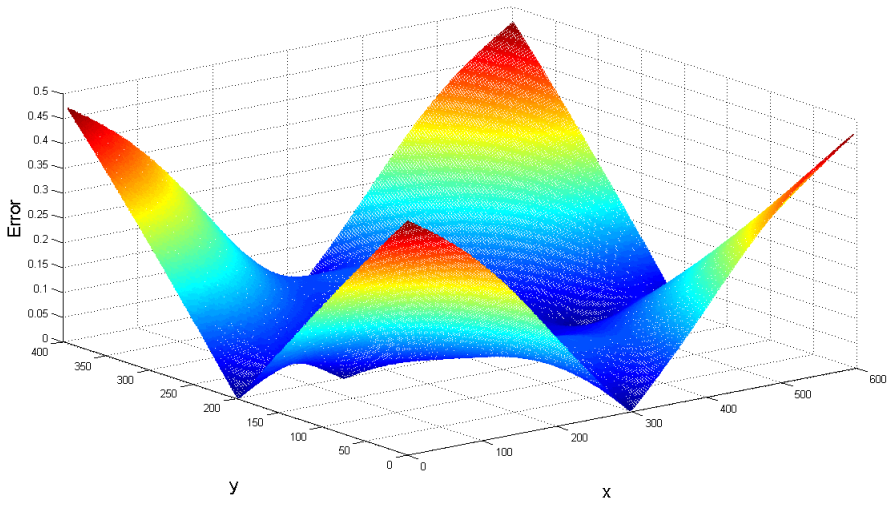

Figure 3.13. WCL performance for case 7 displayed in Figure 3.11b.

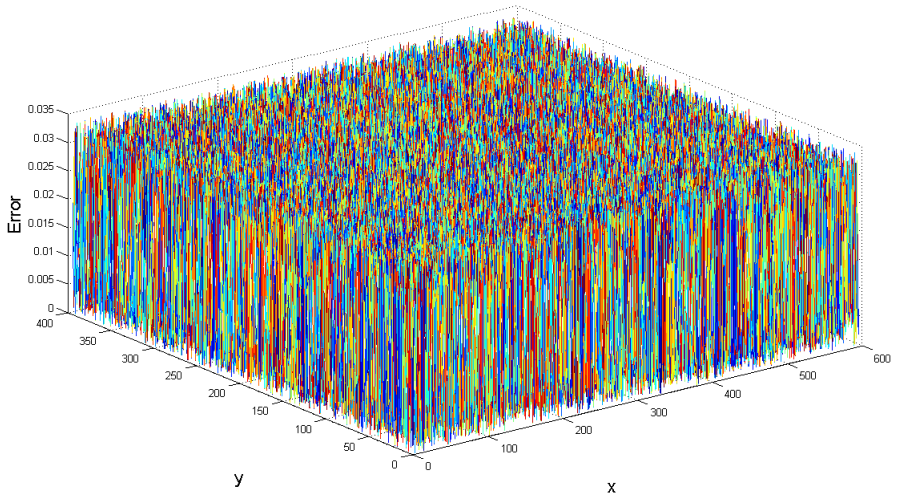

Figure 3.14. Trilateration performance for the cases displayed in Figure 3.11.

error of Trilateration decreased from 2% to 1.5% although the random noise matrix is kept constant, since the modified Trilateration algorithm takes the average of the results obtained from the four different combinations built by different three beacons sets.

3.4. Evaluation of 8 and 16 Beacons Cases

In order to examine the performances of the two methods for higher number of beacons, we run simulations for eight beacons and 16 beacons cases. Beacon placements are shown in Figure 3.15. Results are shown in Figures 3.16 - 3.19.

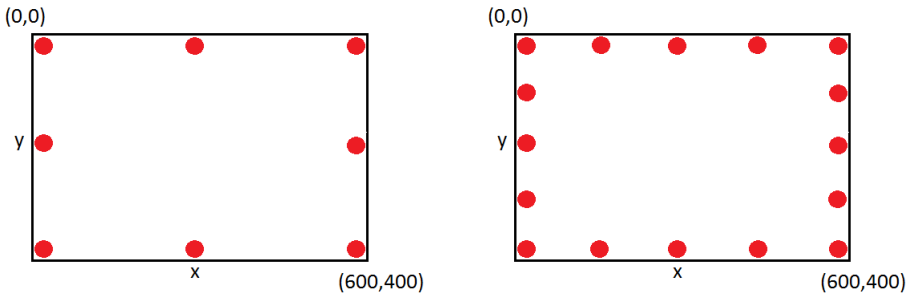

(a) Beacon placement case 8. (b) Beacon placement case 9.

Figure 3.15. Placements of the beacons in eight and 16 beacons cases.

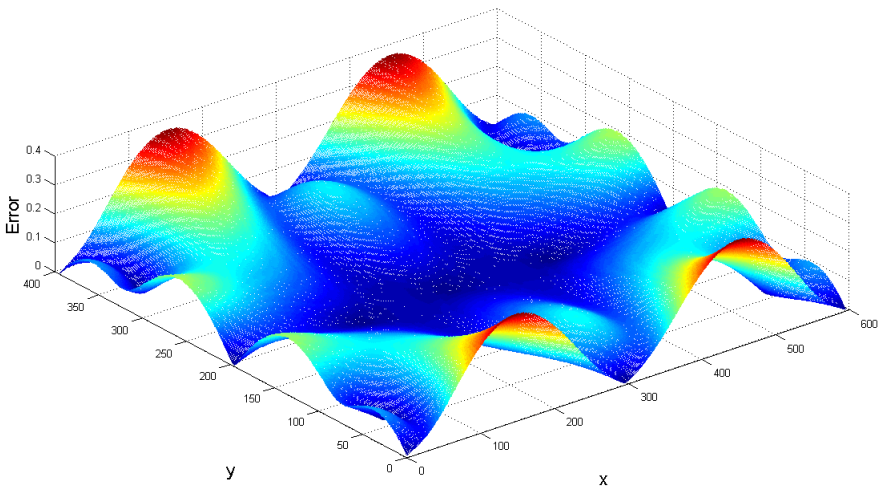

Figure 3.16. WCL performance for case 8 displayed in Figure 3.15a.

Also simulation results displayed in Figures 3.16 and 3.17 show that WCL performance decreases as the node gets closer to the centroid of two consecutive beacons located on a common edge of the simulation field, as seen in the previous cases. The mean error also decreases as the number of beacons is increased, such that mean error

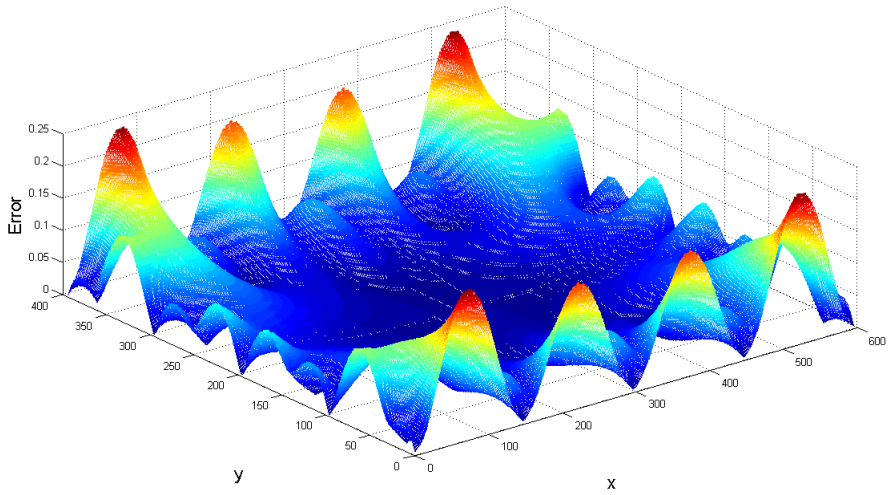

Figure 3.17. WCL performance for case 9 displayed in Figure 3.15b.

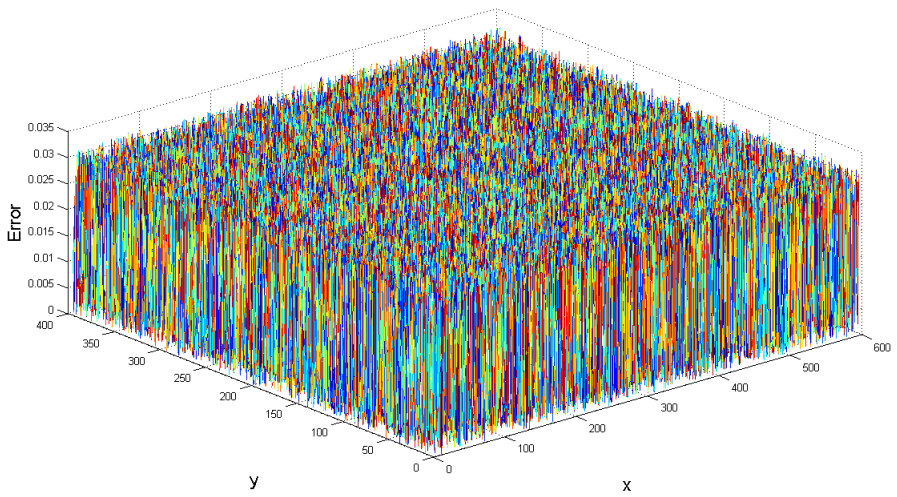

Figure 3.18. Trilateration performance for case 8 displayed in Figure 3.15a.

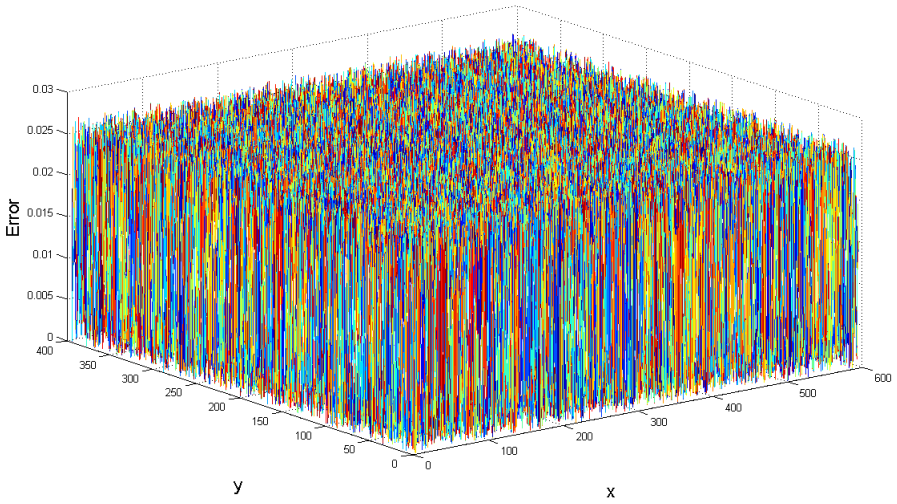

Figure 3.19. Trilateration performance for case 9 displayed in Figure 3.15b.

for the eight beacons case (placement case 8 displayed in Figure 3.15a) is found as 11% while the mean error for the 16 beacons case (placement case 9 displayed in Figure 3.15b) is found as 4.3%. The mean estimation error of the Trilateration also decreased from 1.4% for the eight beacons case to 1.2% for the 16 beacons case.

3.5. Evaluation of the Trilateration and WCL with Erroneous Channel Model

All the simulations up to now are performed assuming that the estimated distances between the node and the beacons are only exposed to random noise, which could be lowered by increasing the number of Monte Carlo iterations. In order to get a better knowledge about performance of both two position estimation methodologies, we modified our simulation software in order to calculate the distances as if they are derived from the ITU Model (see Section 2.2.1.4). We assigned the floor loss penetration factor parameter ($P_f(n)$) of the ITU Model with varying error rates, and observed the performances of WCL and Trilateration methods. Simulations are run for the beacon placement case 6 (see Figure 3.11a). Results are shown in Figures 3.20 - 3.23.

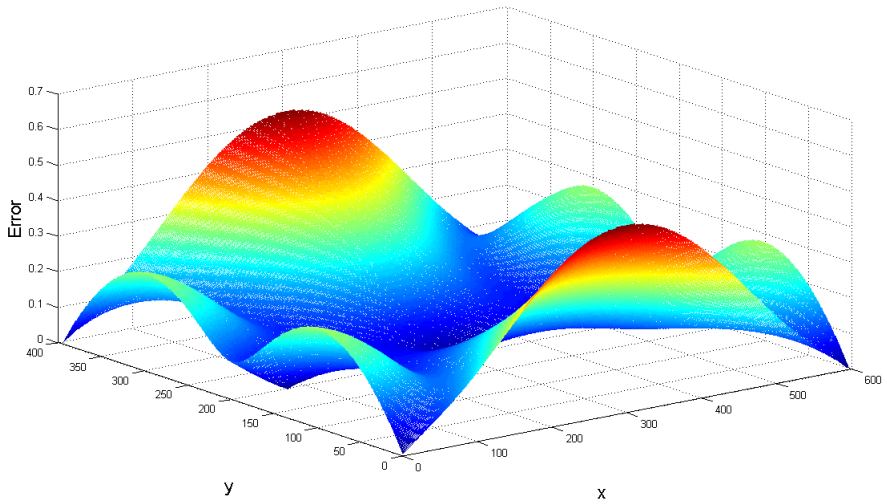

Figure 3.20. WCL performance with the ITU Model, $P_f(n)$ parameter of which is provided with 20% error.

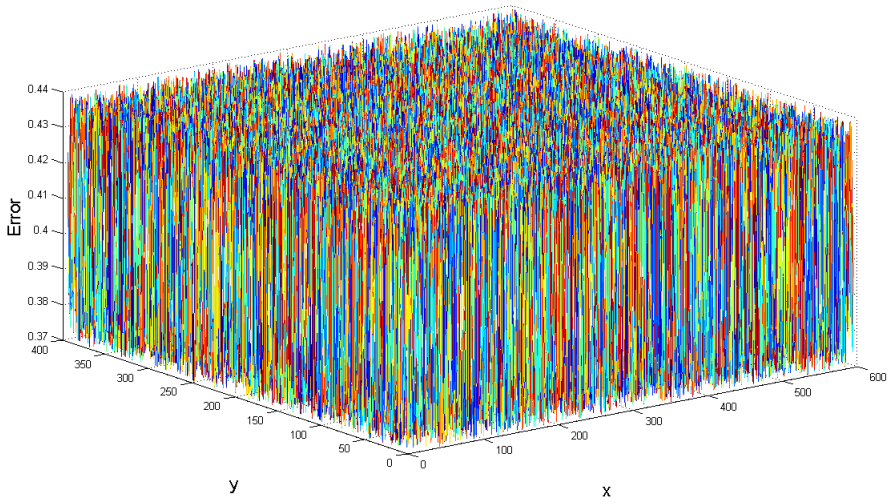

Figure 3.21. Trilateration performance with the ITU Model, $P_f(n)$ parameter of which is provided with 20% error.

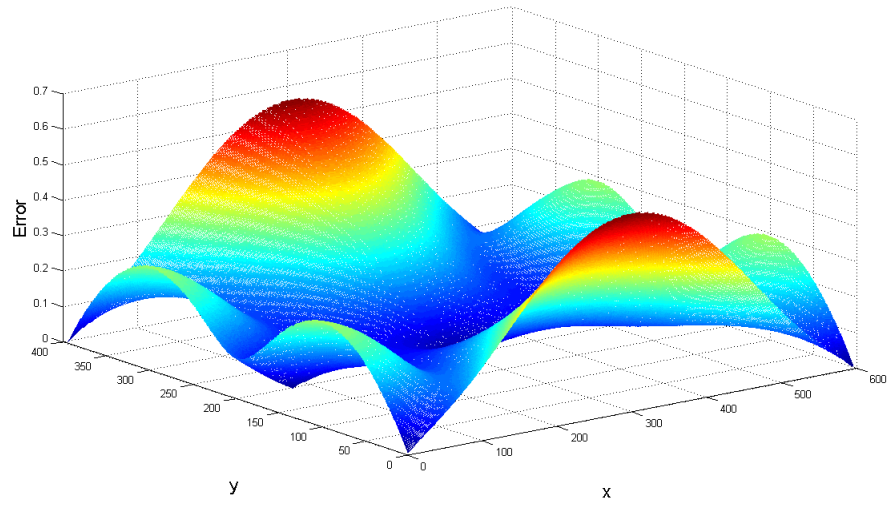

Figure 3.22. WCL performance with the ITU Model, $P_f(n)$ parameter of which is provided with 100% error.

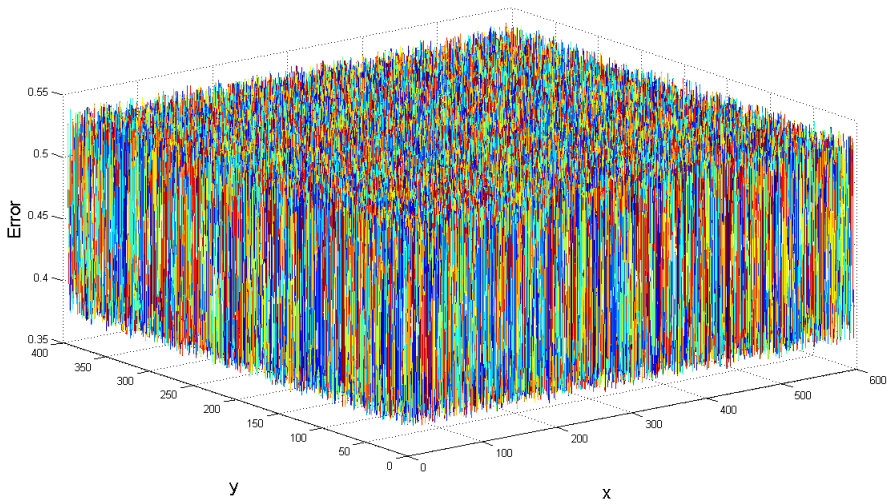

Figure 3.23. Trilateration performance with the ITU Model, $P_f(n)$ parameter of which is provided with 100% error.

3.6. Comparison of WCL and Trilateration Based on the Implemented Simulations

To make a reasonable comparison between the WCL and the Trilateration methods, we simulated them on the same test setup with the same noise vector. Scenarios with 3, 4, 8 and 16 beacons with various placements are implemented. We also simulated the case where one of the channel model parameters is provided with error.

Considering the simulation results displayed in Figures 3.5 - 3.9, one can easily conclude that WCL fails with high error rates with three beacons. It is also seen that WCL performs worse when the beacons are located at the centroids of the sides of the 2-D field (see Figure 3.13). This can be explained by the claim that the WCL algorithm fails when the node position to be estimated is outside of the boundaries set by the beacons. Moreover, estimation error of WCL algorithm increases as the node gets closer to any of the edges of the 2-D field, especially as it gets closer to the centroid of two consecutive beacons. It is also seen that the region on the 2-D simulation field where the error is less than 2%, expands as the number of beacons increases. Furthermore, maximum estimation error encountered decreases as the number of beacons increases. For instance the maximum error is 52% for the beacon placement case 6 (see Figure 3.12), while it is 23% for the beacon placement case 9 (see Figure 3.15b). On the other hand, it is seen in Figures 3.10, 3.18, 3.19 and 3.14 that the Trilateration is quite robust against the number and placements of the beacons, such that the estimation error does not exceed 5% for any of the cases in question.

Simulation results displayed in Figures 3.12, 3.13, 3.16 and 3.17 show that the position estimation performance of the WCL algorithm decreases as the node gets closer to the edges of the 2-D simulation field, especially as the node location gets closer to the centroid of two consecutive beacons. Besides, considering the simulation results displayed in Figures 3.20 - 3.23, one can easily conclude that WCL method is much more robust against errors in the path loss model used in distance estimations, when compared to the Trilateration method, since the estimation error of the WCL algorithm stays nearly constant even if the parameter $P_f(n)$ is assigned with error rates

up to 100%, while the Trilateration performance decreases excessively when erroneous $P_f(n)$ is provided.

Thus, it can be concluded that Trilateration is more robust against varying number and locations of the beacons, while WCL is more dependent on the beacon numbers and placements. On the other hand, WCL is much more robust against errors in channel modelling when compared to the Trilateration.

3.7. Summary of the Chapter and Concluding Remarks

In this chapter, we run simulations for a better understanding of two position estimation methods. We examined the effect of number and placements of the beacons on the position estimation performances of both methods. We also simulated the cases where a parameter of the channel model is provided with different error rates and observed the performance of both methods. Considering the simulations, we have concluded that the Trilateration provides more successful estimates when the channel model perfectly matches with the actual transmission medium. Besides, the WCL method is much more robust against channel model errors. In addition, we have concluded that the Trilateration method is more robust against the beacon number and placements when compared to the WCL method.

4. EXPERIMENTAL EVALUATION OF LOCALIZATION METHODS

In this chapter, we introduce our position estimation system, including the design procedures and performance comparison with the ITU Indoor Channel Model. Initially we designed a ZigBee based path loss measurement system composed of a transmitter and a receiver connected to the PC. Subsequently we collected path loss data in an indoor area. Based on the collected path loss data we derived an indoor path loss model and performed position estimations with both WCL and Trilateration methods.

4.1. Development of the Path Loss Measurement System

In this part we design an RSSI measurement system and give a brief overview about the ZigBee.

4.1.1. Hardware Design

In order to design an empirical indoor path loss model, it is required to collect path loss measurements. To this end, we have designed a ZigBee based RSSI transmitter circuit to communicate with a ZigBee Receiver (see Figure 4.1). The designed transmitter operates with +9V battery. There are two integrated voltage regulators operating in the circuit. One of them is LM7805 and responsible for converting down the input voltage to 5V, which is an appropriate voltage level for the microcontroller and the LED indicators. The other voltage regulator, the UTC1117, converts the 5V output of the LM7805 down to 3.3V, which is the operating level for the ZigBee modem. The microcontroller communicates with the ZigBee modem through its UART port to send the RSSI data in ZigBee frames to the ZigBee receiver. Since the logic levels of the microcontroller and the ZigBee device are different from each other, there are voltage divider resistors between the UART ports of the microcontroller and the ZigBee device. Thus, the data output of the microcontroller is attenuated to the logic

Figure 4.1. ZigBee receiver module.

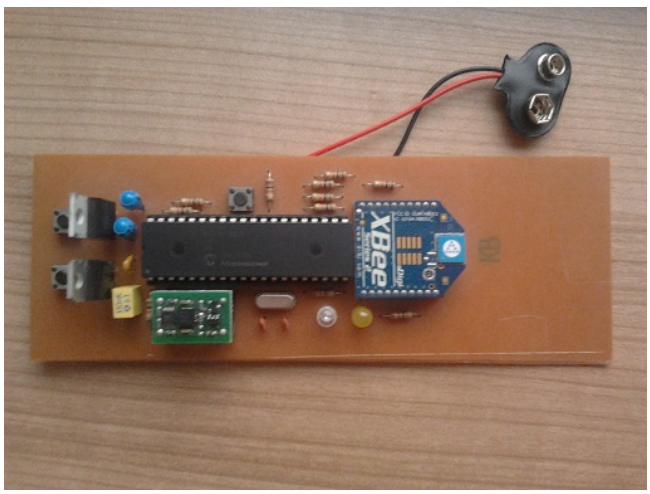

Figure 4.2. RSSI transmitter.

high level of the ZigBee device, which is 3.3V. On the other hand, the UART output of the ZigBee device is not required to be upconverted to the logic high level of the microcontroller, since logic high level of the ZigBee modem is higher than the logic high to logic low transition threshold of the microcontroller. We used submodules of the Proteus software for the circuit design (ISIS for the circuit diagram, ARES for the PCB schematic). PCB schematic and circuit diagram of the RSSI transmitter are shown in Figures 4.3 and 4.4, respectively. RSSI data reception of the microcontroller from the ZigBee modem is explained in Section 4.1.2.

The ZigBee receiver pushes the RSSI data captured from the RSSI transmitter to the PC via USB. The receiver builds a virtual serial port on the PC. WCL Simulator

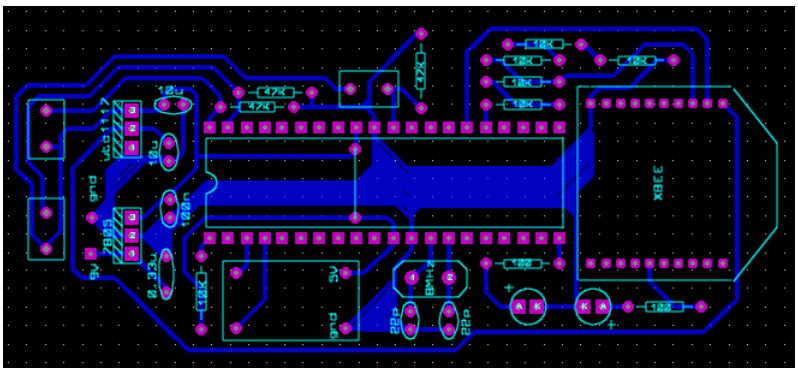

Figure 4.3. PCB schematic of the RSSI transmitter.

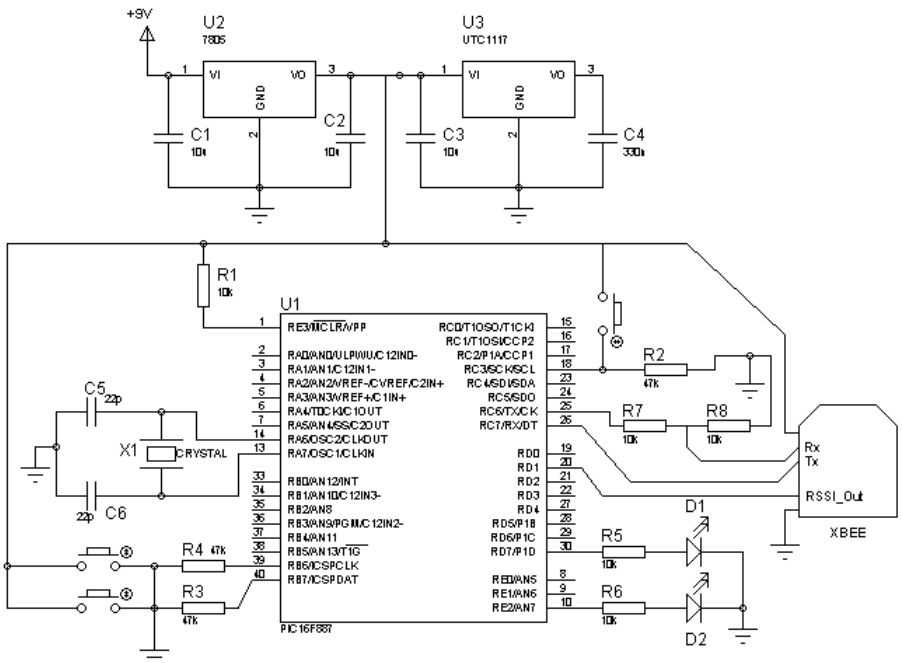

Figure 4.4. Circuit diagram of the RSSI transmitter.

software is updated by developing and adding a new .NET class, in order to communicate with the ZigBee receiver via the virtual serial port acting on the USB port of the PC, where the ZigBee receiver is connected to. Data packages, which contain the RSSI values and pushed from the ZigBee receiver to the PC, are built according to the ZigBee API Frames. Hence, a ZigBee frame decomposer class has been developed and added to the WCL Simulator.

4.1.2. A Brief Explanation of the ZigBee and RSSI Data Reception

ZigBee is a package of data transmission protocols specifically designed for the PAN networks of low-power RF devices based on the IEEE 802 standard [12]. ZigBee provides mesh networking, so that two distant small RF devices could communicate with each other using intermediate ZigBee devices as repeaters. Thus, there is no need for a centralized controller such as a base station covering all the devices in the network. ZigBee devices can be initialized with three types of tasks [12]:

- ZigBee Coordinator (ZC): It acts as the root of the network and can be used as a bridge to another network. A coordinator is unique in a network and the only one which is capable of starting a network.
- ZigBee Router (ZR): It is capable of executing an application in addition to acting as a repeater transmitting received data to the next device on the data transmission path.
- ZigBee End Device (ZED): It is the most economical device of the network from the power consumption point of view, since it is capable only of talking to the parent device, which can either be a Coordinator or a Router.

We used the XBee modules of MaxStream as the ZigBee modems (see Figure 4.5). The XBee RF modules are able to communicate with any device through its UART port. The module has an RSSI/PWM pin which outputs a PWM signal indicating the signal strength of the last received data packet. The command "P0" is used to enable the RSSI/PWM output of the pin. Setting "P0" to 1 makes the RSSI/PWM

Figure 4.5. MaxStream XBee.

pin output PWM signals, frequencies of which are adjusted depending on the received signal strength values of the received packets. The PWM signal output following a received packet, is enabled for a period of time adjusted by the "RP" command. After each packet reception, a new PWM signal is output and the timer adjusted by the "RP" command is reset. If there is no data received for an amount of time more than the RSSI timer period, then the RSSI/PWM pin is set to low. Default value for "RP" is 40, and it is measured in 100ms units, such that an assigned value of 40 maps to 4 seconds. The output PWM signal runs at 12MHz and has 2400 total counts (200 μs period).

In order to get RSSI values from the module as described above, it is needed to activate the RSSI data provider block of the module, which requires to enter the command mode and modify the related register. To Enter AT Command Mode; we send the 3-character command sequence "+++" and observe guard times before and after the command characters. After 1 second duration the module responds by sending an "enter" character, corresponding Ascii value of which is 13, out of the data out pin, indicating that the command mode has been initiated. Then the P0 register is set by sending data according to the frame displayed in Figure 4.6.

If the sent command frame is correct, then the module will respond by sending the "OK" message. Otherwise the module returns the "ERROR" message. It is also necessary to remind that all the sent and received messages are the corresponding Ascii values of the message characters. After the module informs that P0 activation request is successful, it is needed to send "apply changes" command, Ascii command of which corresponds to the string "AC".

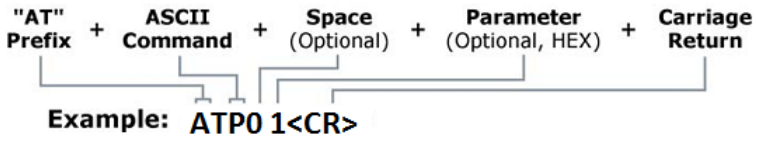

Figure 4.6. Command format for setting the RSSI data provider.

4.1.3. Data Collection

After completing the hardware design and software update procedures, RSSI measurements, as a requirement for our empirical indoor channel model design are implemented in a 20 meters x 50 meters closed area. The ZigBee receiver together with a PC are placed to a corner of the stated closed area, and then we moved RSSI transmitter along the diagonal of the area (54 meters) sending 200 RSSI samples per 1 meter. Data collection procedure is as follows: ZigBee receiver frequently broadcasts dummy packages. As a broadcast package is received by the XBee module on the RSSI transmitter, it sends a PWM signal to the microcontroller, frequency of which is a function of the RSSI value of the last received data packet. The microcontroller extracts the RSSI value (1 byte), and then builds and sends a frame to the ZigBee receiver containing the received RSSI byte. ZigBee receiver pushes the frame to the PC, in order for the updated WCL Simulator to decompose the frame to get the RSSI byte. Once the RSSI byte is received by the WCL Simulator, it is than converted to path loss in dB as follows: The RSSI data output from the XBee module is in [dBm], hence the received power can be derived from Equation 2.19 by assigning $P_{Ref} = 1mW$. Once the received power is derived, than the corresponding path loss value is generated by Equation 2.1. The path loss vs distance plot of our measurements is shown in Figure 4.7.

We also tested the correlation of the ITU Model with our measurements. The corresponding ITU Model for the same floor case is as

$$PL(d) = 39.6 + 30 \cdot \log(d) \tag{4.1}$$

where $PL(d)$ is the path loss in dB, and d is the distance in meters.

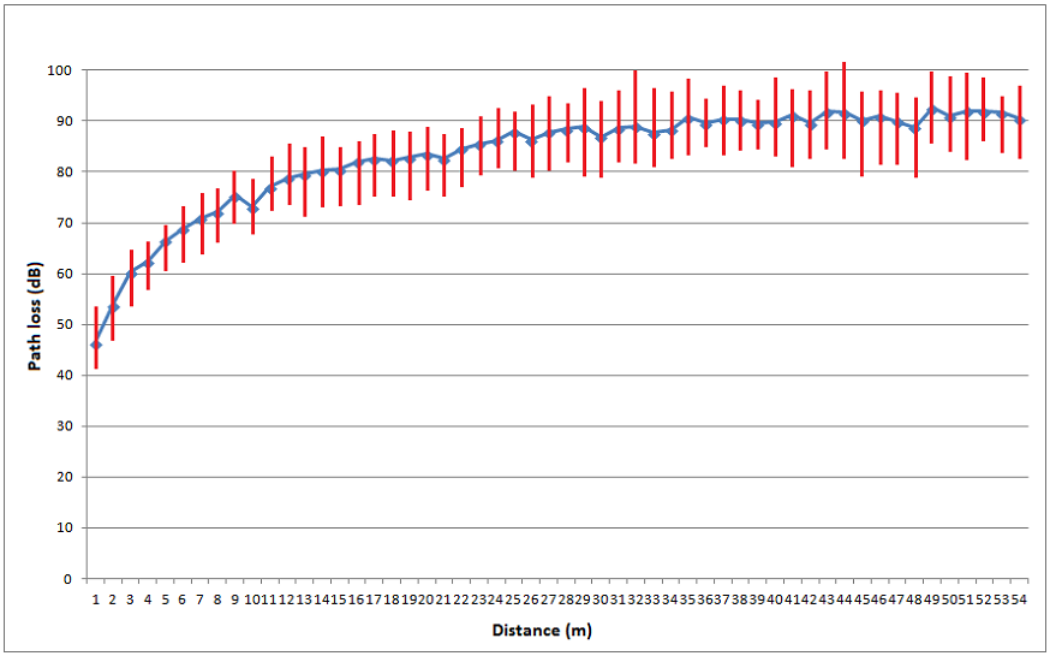

Figure 4.7. Path loss vs distance (The blue dots and the red bars represent the average path loss and the variation of the path loss measurements at the related distances, respectively).

ITU Model estimations and the measurements are displayed together in Figure 4.8. It can easily be concluded from Figure 4.8 that the ITU Model performance is not satisfactory in the industrial area, where we collected our measurement data.

4.2. Empirical Channel Model Design

We have derived an empirical log distance path loss model based on our measurements and the generic log distance model, which is expressed as

$$L(d) = L(1) + \eta \cdot \log(d) \tag{4.2}$$

By rewriting Equation 4.2 as

$$L(d) - L(1) = \eta \cdot \log(d) \tag{4.3}$$

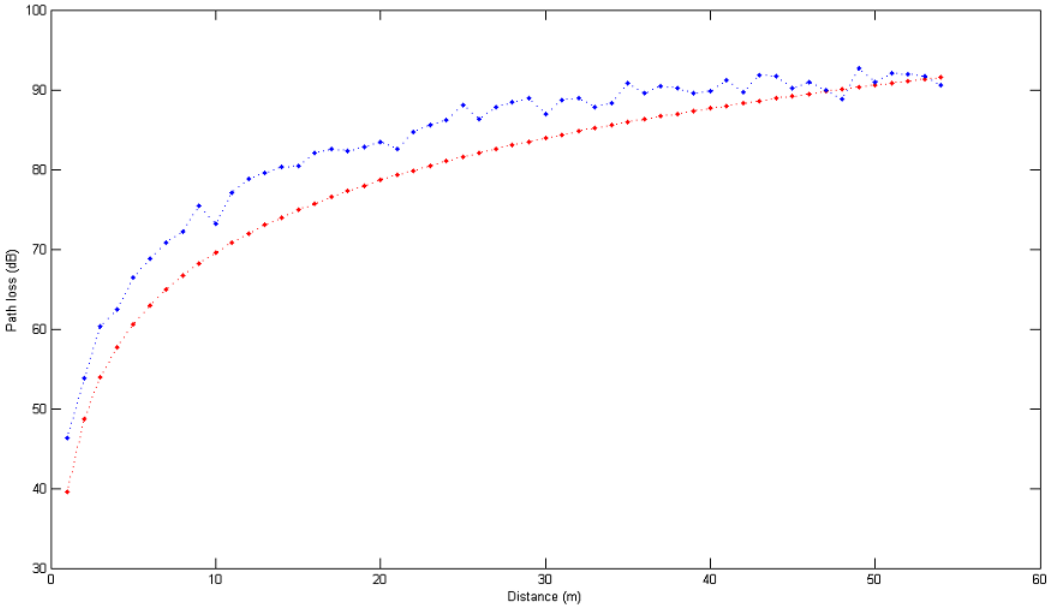

Figure 4.8. ITU Model path loss estimations vs our measurements (The red curve and the blue plot represent the theoretical path loss estimations of the ITU Model and the measured path loss values, respectively).

and considering the distances varying between 1 meter and 54 meters (d_1 through d_{54} = 1m through 54m), we can represent Equation 4.3 in matrix form:

$$\begin{bmatrix} \log(2) \\ \vdots \\ \log(54) \end{bmatrix} \cdot \eta = \begin{bmatrix} L(2) \\ \vdots \\ L(54) \end{bmatrix} - \begin{bmatrix} L(1) \\ \vdots \\ L(1) \end{bmatrix}$$

By letting

$$A = \begin{bmatrix} \log(2) \\ \vdots \\ \log(54) \end{bmatrix}, b = \begin{bmatrix} L(2) - L(1) \\ \vdots \\ L(54) - L(1) \end{bmatrix}$$

we obtain the system of

$$A \cdot \eta = b \tag{4.4}$$

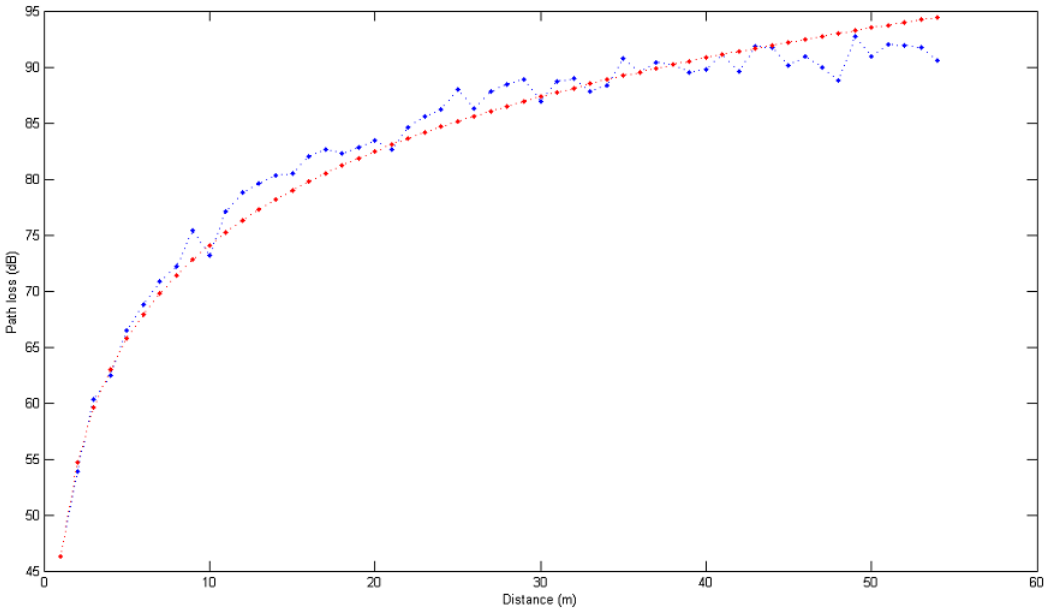

Figure 4.9. Predictions of our path loss model vs measured path loss values (The red curve and the blue plot represent the theoretical path loss estimations of our model and the real path loss measurements, respectively).

The least squares solution of the above system is given by

$$\eta = (A^T A)^{-1} \cdot A^T b = \frac{\sum_{i=2}^{54} \log(i) \cdot [L(i) - L(1)]}{\sum_{i=2}^{54} \log^2(i)} \tag{4.5}$$

The numerical value of Equation 4.5 for the data yields

$$\eta = 27.7753 \tag{4.6}$$

Noting that the path loss at reference distance 1m is measured as $L(1) = 46.3118$, our path loss model is thus finalized as:

$$L(d) = 46.3118 + 27.7753 \cdot \log(d) \tag{4.7}$$

Figure 4.9 displays the performance of our path loss model when compared with the real path loss measurements.

4.3. Position Estimation Implementations Based on the Designed Model

After completing the design procedures, we tested our path loss model in position estimations by using path loss values corresponding to distances of all the possible positions to where the ZigBee receiver is placed. Since we could not obtain enough number of ZigBee modules, we tested our model on the WCL Simulator, and the Trilateration tool we generated in Matlab. We made the simulations using both WCL and Trilateration methods for the beacon placement case 6, by setting the simulation field dimensions to 20 x 50.

At each step of the simulations, once the distance between the node and a beacon is calculated, then the corresponding path loss value obtained from our measurements to the calculated distance, is input to our model. Then the distances output from our model are used in position estimations, as explained in previous sections.

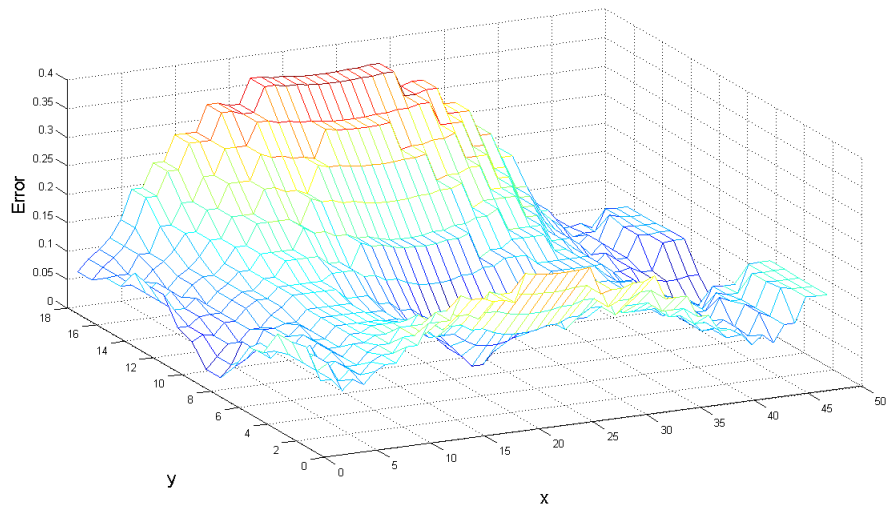

Figure 4.10. Position estimations performed by our path loss model with the WCL method.

Considering the results shown in Figures 4.10 and 4.11 we see that the overall performance of WCL has a minor difference when compared to running the algorithm with ideal distance values. But the case is worse for the Trilateration simulations, such

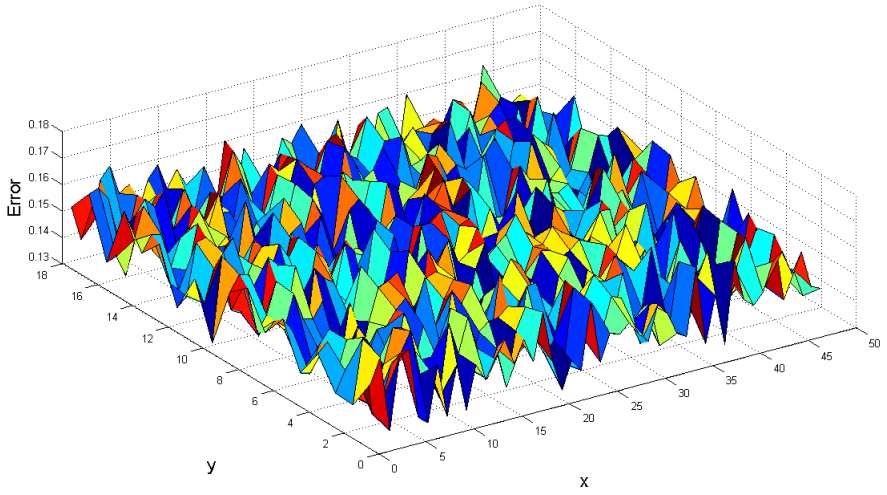

Figure 4.11. Position estimations performed by our path loss model with the Trilateration method.

that the error is about 16%, supporting our assertion that the Trilateration method is much more dependent on the errors in the channel model parameters.

4.4. Summary of the Chapter and Concluding Remarks

This chapter summarizes the experimental test bed we have developed to collect path loss data in an indoor area. Based on the collected path loss data, we built our empirical indoor channel model, using the Least Squares approach for fitting our Log-Distance based curve on the collected path loss data with minimum error. After completing the channel model design, we tested our model with both the Trilateration and the WCL methods. Both methods have advantages and drawbacks against each other which are handled in previous sections, but based on the tests for the beacon placement case 6 (see Figure 3.11a), WCL performed better than the Trilateration method (see Figures 4.10 and 4.11).

5. CONCLUSION

In this thesis, a 2-D indoor position estimation system is designed and implemented following the design of a log-distance based empirical indoor channel path loss model for ZigBee sensor networks using the path loss data measured in an industrial area. The designed model is realized by applying curve fitting on the path loss measurements using the Least Squares Solution method. The performance of the designed model is compared with the ITU model for indoor attenuation. Based on the collected path loss data, our model gives obviously more successful distance estimates. We also compared the position estimation methods which are the WCL and the Trilateration, with simulations based on both the exact distances exposed to Gaussian noise, and the distance estimation results of our model. It is concluded that; under the same noise characteristics, Trilateration method gives more precise position estimates compared to the WCL, if all the parameters of the channel model are known with no error. In contrast, WCL is much more robust against errors in the channel model parameters, when compared to the Trilateration. Hence, WCL will be a better choice unless the path loss based distance estimating channel model perfectly matches with the real channel model of the indoor area in question. Future work will concentrate on designing a 3-D position estimation system for multi-floored buildings.

REFERENCES

1. Mardeni, R. and S. N. Othman, "Node Positioning in ZigBee Network Using Trilateration Method Based on the Received Signal Strength Indicator (RSSI)", *European Journal of Scientific Research*, Vol. 46, pp. 48–61, 2010.

2. Goldsmith, A., *Wireless Communications*, Cambridge University Press, California, CA, USA, 2005.

3. Hameed, S. M., "Indoor Propagation Modeling for Wireless Local Area Network (WLAN)", *International Journal of Computers, Communications and Control (IJCCC)*, Vol. 11, 2011.

4. Serodio, C., L. Coutinho, L. Reigoto, J. Matias, A. Correia and P. Mestre, "A Lightweight Indoor Localization Model Based on Motley-Keenan and COST", *Proceedings of the World Congress on Engineering*, Vol. 2, London, U.K, 2012.

5. Lott, M. and I. Forkel, "A Multi-Wall-and-Floor Model For Indoor Radio Propagation", *Vehicular Technology Conference, 2001. VTC 2001 Spring. IEEE VTS 53rd*, Vol. 1, pp. 464–468, Rhodes, 2001.

6. Kaminsky, A., *Trilateration*, Lecture note, Rochester Institute of Technology, 2007.

7. Blumenthal, J., R. Grossmann, F. Golatowski and D. Timmermann, "Weighted Centroid Localization in ZigBee-based Sensor Networks", *IEEE International Symposium on Intelligent Signal Processing*, pp. 1–6, Alcala de Henares, 2007.

8. Bulusu, N., J. Heidemann and D. Estrin, "GPS-less Low Cost Outdoor Localization For Very Small Devices", *IEEE Personal Communications*, Vol. 7, pp. 28–34, 2000.

9. Jang, W. S. and M. J. Skibniewski, "A Wireless Network System for Automated Tracking of Construction Materials on Project Sites", *Journal of Civil Engineering*

and Management, pp. 11–18, 2008.

10. Saxena, M., "Experimental Analysis of RSSI-Based Location Estimation in Wireless Sensor Networks", *3rd International Conference on Communication Systems Software and Middleware and Workshops, COMSWARE*, pp. 503–510, Bangalore, 2008.

11. Seidel, S. Y. and T. Rappaport, "914 Mhz Path Loss Prediction Models for Indoor Wireless Communications in Multifloored Buildings", *IEEE Transactions on Antennas and Propagation*, Vol. 40, pp. 210–211, 1992.

12. Pekhteryev, G., Z. Sahinoglu, P. Orlik and G. Bhatti, "Image transmission over IEEE 802.15.4 and ZigBee networks", *IEEE International Symposium on Circuits and Systems, 2005. ISCAS 2005.*, Vol. 4, pp. 3539–3542, Kobe, Japan, 2005.